ANALYSIS OF WIND TURBINE HUB COMPONENT

by

HAMZA KAZANCİ

Submitted to the Graduate School of Engineering and Natural Sciences

in partial fulfillment of

the requirements for the degree of

Master of Science

Sabancı University

November 2014

ANALYSIS OF WIND TURBINE HUB COMPONENT

APPROVED BY:

Assoc. Prof. Dr. Mahmut F. AKŞİT .....

(Thesis Advisor)

Assoc. Prof. Dr. Ali Koşar .....

Assoc. Prof. Dr. Ilyas Kandemir .....

DATE OF APPROVAL: 03.11.2014

ANALYSIS OF WIND TURBINE HUB COMPONENT

Hamza KAZANCİ

Mechatronics Engineering, MS Thesis, 2014

Thesis Advisor: Assoc. Prof. Dr. Mahmut F. AKŞİT

Keywords: Wind Turbine, Hub, Structural Analysis, Rotor

ABSTRACT

Wind energy has become one of the most popular renewable energy sources in the last few decades due to renewed awareness for environmental issues. Pollution and global warming are the most significant problems in the world. Many wars have been made to control and possess energy resources. Environmental issues caused by fossil energy production facilities have attracted attention to global warming, air and water pollution in recent years. Therefore, governments and universities encourage research and development efforts in wind turbine technology to achieve more efficient turbines with less cost. Wind turbine technology became of the most important engineering subjects in recent years.

In this thesis, the analysis of the rotor hub of a 500 kW prototype wind turbine has been conducted. The hub has been modeled and meshed using commercially available code HyperMesh. The hub is modeled with its neighboring components to achieve a more realistic and detailed simulation. 3D design has been created in SolidWorks. Contacts and loads have been defined using commercially available finite element code ABAQUS. In other words, modeling process has been completed in ABAQUS. Structural analysis has been performed for two different scenarios which were chosen as the worst case extreme operating conditions. Analysis results have been examined for different perspectives. Especially, stress values and contacts have been considered. Finally, fatigue analyses have been conducted using commercially available code FEMFAT. Reaction of the material against dynamic loading has been examined.

RÜZGAR TÜRBİNİ GÖBEK PARÇASININ ANALİZİ

Hamza KAZANCİ

Mekatronik Mühendisliği, Yüksek Lisans Tezi, 2014

Tez Danışmanı: Doç. Dr. Mahmut F. AKŞİT

Anahtar Kelimeler: Rüzgar Türbini, Göbek, Yapısal Analiz, Rotor

ÖZET

Son yıllarda dünyadaki en önemli sorunlar olan enerji kaynaklarının azalması ve çevresel sorunlar nedeniyle rüzgar enerjisi en popular sektörlerden biri haline gelmiştir. Birçok savaş bile enerji kaynaklarının tükenmesinden ötürü ortaya çıkmıştır. Öte yandan küresel ısınma, hava ve su kirliliğiyle beraber enerji üretim santrallerinden kaynaklı çevresel sorunlar yakın zamanda dikkat çekmektedir. Bu yüzden hükümetler ve üniversiteler rüzgar türbin teknolojisinin daha verimli ve daha az masraflı olması için bu alandaki gelişmeleri teşvik etmektedirler. Son yıllarda rüzgar turbine teknolojisi en önemli mühendislik konularından biri haline gelmiştir.

Bu tez çalışmasında, Türkiye'nin ilk yerli rüzgar türbininin rotor göbek parçasının analizi incelenmiştir. Parça daha gerçekçi ve detaylı olması için Hypermesh yazılımında komşu komponentleriyle beraber SolidWorks yazılımında hazırlanan 3D dizaynına uygun olarak örgülenmiştir. Temas bölgeleri ve yüklemeler ise ABAQUS yazılımında tanımlanmıştır. Diğer bir deyişle modelleme süreci ABAQUS yazılımnda tamamlanmıştır. En kötü olarak seçilen iki farklı senaryonun yapısal analizi aynı yazılımda gerçekleştirilmiştir. Analiz sonuçları çok farklı açılardan incelenmiştir. Özellikle gerilme değerleri ve temas yüzeyleri göz önünde bulundurulmuştur. Son olarak bu modellerin yorulma analizleri FEMFAT yazılımı tarafından gerçekleştirilmiştir. Burada ise malzemenin dinamik yükler altındaki reaksiyonu incelenmiştir.

“To my family and fiancée…”

ACKNOWLEDGEMENTS

I wish to express my sincere thanks to Assoc. Prof. Dr. Mahmut F. Akşit, more than my thesis advisor, for his precious advice and unexampled guidance of this work. I am thankful to him not only for the completion of this thesis, but also for his unending enthusiasm in all matters of life. I also wish to thank Assoc. Prof. Dr. Ali Koşar and Assoc. Prof. Dr. İlyas Kandemir for being my thesis committee.

I would like to thank to my parents and my sisters for their great confidence in me, their understanding like an ocean, supporting me in whatever my decisions are and making me always feel them near.

I would also like to thank all of my friends at Sabancı University. Especially, I would like to thank Gökay Çoruhlu, Hasan Azgın, Ömer Seçmeler, Barış Arseven and Ali Celaleddin Gemci all of who make my student years more valuable and entertaining for me with their sincere friendship and pleasant conversation.

I cannot pass my high school friends Furkan Gençalioğlu, Ebubekir Karagöl, Mustafa Çuha and Mücahit Coşkun wihout expressing my great thanks for making Istanbul as my hometown and never-ending friendship.

I want to express my sincere thanks to Caner Akcan, Ercan Akcan, Murat Koyuncuoğlu, Abdullah Çar and Rıdvan Rafi Akşit who I had a chance to work together.

I would like to acknowledge the support provided by The Scientific & Technological Research Council of Türkiye (TÜBİTAK) during my master studies.

Finally, I wish to convey my special thanks to my fiancée for supporting me every time, great understanding and confidence in me, endless patience and encouragement during my education. Thank you for being in my life.

TABLE OF CONTENTS

LIST OF FIGURES

LIST OF TABLES

LIST OF SYMBOLS

A	:	Area which is exposed to wind
C_p	:	Power coefficient
D	:	Rotor diameter
E	:	Energy
F_t	:	Outer plane cutting force
F_y	:	Inner plane cutting force
H	:	Tower height
L	:	Length in wind direction
m	:	Mass
$\dot{m}$	:	Mass flow
M_x	:	Inner plane moment
M_y	:	Outer plane moment
M_z	:	Torsional moment
n	:	Amount of gas molecules
P	:	Gas pressure
ρ	:	Density
R	:	Universal gas constant
t	:	Time
T	:	Temperature
v	:	Velocity
V	:	Volume
V_0	:	Wind speed

LIST OF ABBREVIATIONS

COPEN	:	A module in ABAQUS to examine contact opening
CSTATUS	:	A module in ABAQUS to examine contact status
EN-GJS-400-18-LT	:	Spheroidal graphite cast iron
HAWT	:	Horizontal-axis wind turbine
MILRES	:	National Wind Energy Systems Development and Prototype Turbine Production
VAWT	:	Vertical-axis wind turbine

1. INTRODUCTION

The effect of depleting energy resources on our daily life is increasing day by day. Many wars occur to control limited energy resources around the world. As pollution and depletion of fossil energy resources push scientists to search for alternatıve energy resources, the concept of "renewable energy" has been gaining ever increasing importance is increasing in recent years.

Using wind energy in electricity production has gained wide acceptance with mass industrial production and increase in turbine unit power. Therefore, there is increasing need to establish deep and detailed information about wind turbine, design, production and management.

When wind turbine design is considered, there are many turbine components that require special attention such as blades, hub, tower, gearbox, generator… Especially, blades and hub are the most important mechanical components in turbine design as they are subjected to the most critical aerodynamic and structural loads. There are some critical considerations in the design process;

- Excessive loading and resistance to fatigue,
- Optimum conical angle to avoid blade/tower collision,
- Avoiding resonance,
- Preferably, low weight and low cost.

There are various types of wind turbines. The most common type is three blade horizontal axis wind turbine systems. These turbines include different components. One of the most crucial components is rotor system which includes blades, hub, slewing bearings and servo motors. Considering the quantity, strength, castability and cost trade off ductile iron grade EN-GJS-400-18-LT is used for majority of wind turbine parts. This material can withstand the possible wind forces and long-term exposure to the environment without failure [12]. In this thesis, structural analyses have been conducted using the mechanical properties of the hub material EN-GJS-400-18-LT. Finite element analyses have been performed using various commercially available software programs. 3D hub design has been created using SolidWorks. Finite element model and mesh have been prepared using HyperMesh. Finally, finite element analyses have been conducted using ABAQUS and fatigue analyses have been performed using FEMFAT.

1.1. Problem Statement

In the literature, there is not much published information about wind turbine hub analysis. Most of these works involve structural analyses. This work aims to identify critical regions of a hub for a 500 kW wind turbine prototype. The worst two load case scenarios have been picked among many different pitch angles. The reason for the analyses to be performed using these two extreme cases is not to determine fatigue factor of safety, rather to identify critical regions for fatigue failure during experimental operation of the prototype. These locations will be equipped with strain gauges and their load cycles will be closely monitored until the design is validated.

Structural analyses have been conducted for these worst case situations. Moreover, blade connecting rings and shaft of the wind turbine have been added to simulation to obtain more realistic results. Wind loads and moments have been applied on the blade connecting rings.

2. BACKGROUND

This work has been conducted as part of National Wind Energy Systems Development Project. As part of the project scope, a 500 kW wind turbine prototype has been studied during the initial phase of the project. This work contains analysis and study of various design scenarios for a sample hub design.

2.1. Definition

Wind turbines convert kinetic energy of the wind to electrical energy. Wind energy is called as green technology. In recent years, interest on the wind turbines is increasing drastically due to its environmental specifications. There are two types of wind turbines which are grouped with respect to their working principles as fixed and variable speed. Variable speed wind turbines are mostly preferred today due to its efficiency. In this project, aimed output is a 500kW wind turbine with fixed speed, but variable blade pitch and turbine direction.

2.2. Wind Resource

A wind turbine converts kinetic energy to mechanical energy via blades, finally to electrical energy via a generator. The maximum available energy, *E*, is obtained if theoretically the wind speed could be reduced to zero [1].

$$E = \frac{1}{2}\dot{m}V_0^2 = \frac{1}{2}\rho A V_0^3 \tag{1.1}$$

$\dot{m}$ is the mass flow, V_0 is the wind speed, ρ is the density of air and A is the area where the wind speed has been reduced. According to this equation, power increases with the cube of the wind speed, and linearly with density and area. Therefore, the wind speed should be carefully measured over a period before each project.

In real applications wind speed cannot be reduced to zero. Therefore, the ratio between the actual obtained power and the maximum available power is defined as power coefficient C_p according to the given equation. There is a theoretical maximum limit for C_p which is called as Betz limit

$$C_{Pmax} = \frac{16}{27} = 0.593\ . \tag{1.2}$$

Modern wind turbines are optimized to a level that they are operated near the limit such as 0.5. According to statistics on many different turbines in Denmark, approximately 1000 kWh/m^2/year energy is produced [1]. However, as production is very site dependent, this would be a crude estimation and can represent only the sites in Denmark.

In wind turbine design it is more efficient to use the lift force than the simple drag as the main source of propulsion. This has been discovered many years ago by sailors. Lift and drag are the perpendicular and parallel components of the relative wind. Therefore, all modern wind turbines have a number of rotating blades looking like propeller blades. If the blades are connected to a horizontal shaft, the turbine called as horizontal-axis wind turbine (HAWT), and if the shaft is vertical, the turbine is called as vertical-axis wind turbine (VAWT). A horizontal-axis wind turbine is illustrated in Figure 2.1.

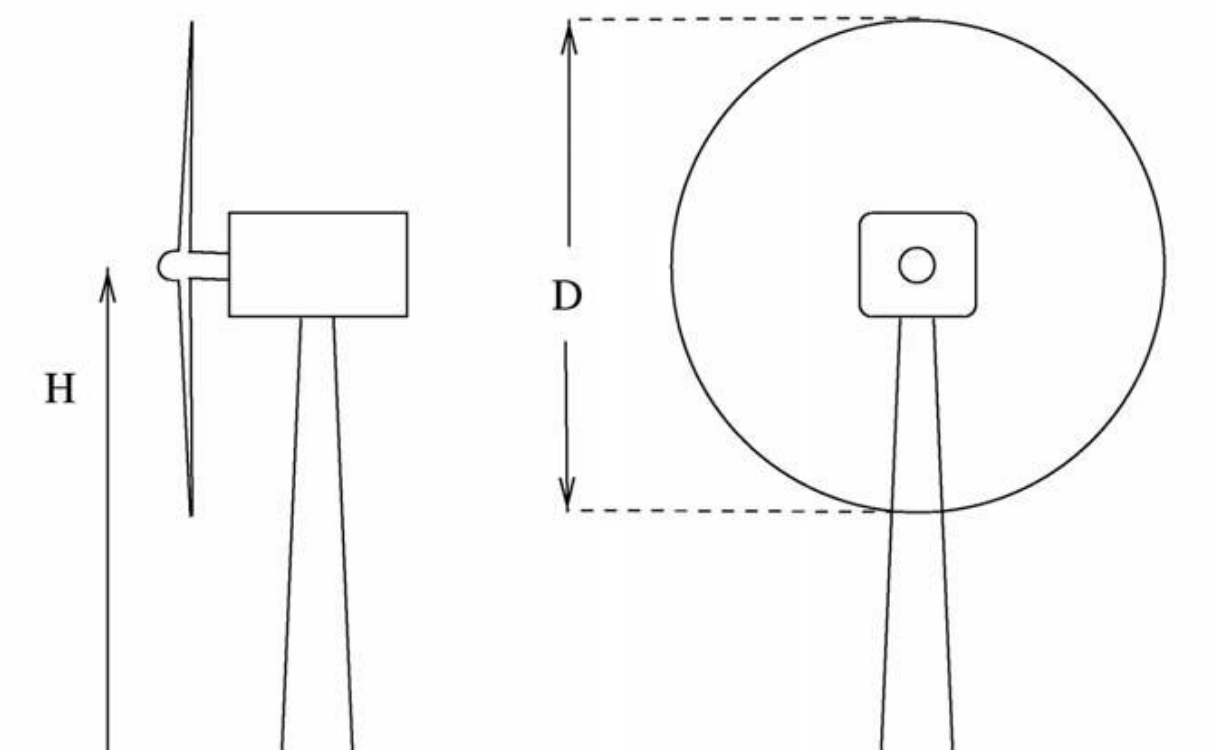

Figure 2.1. Horizontal-axis wind turbine (HAWT) [1]

Wind speed increases with height above the ground and rotor diameter gives the energy collection area. Therefore, the tower height *H* and the diameter *D* are important. The ratio between the rotor diameter *D* and the hub height *H* is generally one. There are generally two or three blades on a modern wind turbine. Wind turbines with two blades are cheaper, but they rotate faster and seem more flickering. However, wind turbines with three blades seem calmer and they are more harmonious to the environment. Three-bladed wind turbines are more efficient aerodynamically than the two-bladed wind turbines. A wind turbine with two blades is generally a downwind machine. The shaft connection is flexible and the rotor is mounted on the shaft via a hinge. This setup is called as teeter mechanism and bending moments are not transferred from the rotor to the mechanical shaft. This type of construction is more flexible than the stiff three-bladed rotor and some components can be built lighter and smaller, which therefore reduces the cost of the wind turbine. Downwind turbines are noisier than upstream turbines as revolution of each blade is heard as low frequency noise.

The rotational speed of a wind turbine rotor is approximately 20 to 50 rpm. Direct drive turbines have low speed generators rotating at the same speed as the blade rotor.

However, in common wind turbines with gear box the rotational speed of most generator shafts is approximately 1000 to 3000 rpm. A gearbox must be used between the low-speed motor shaft and the high-speed generator shaft. An offshore wind turbine which is designed by Siemens is showed in Figure 2.2.

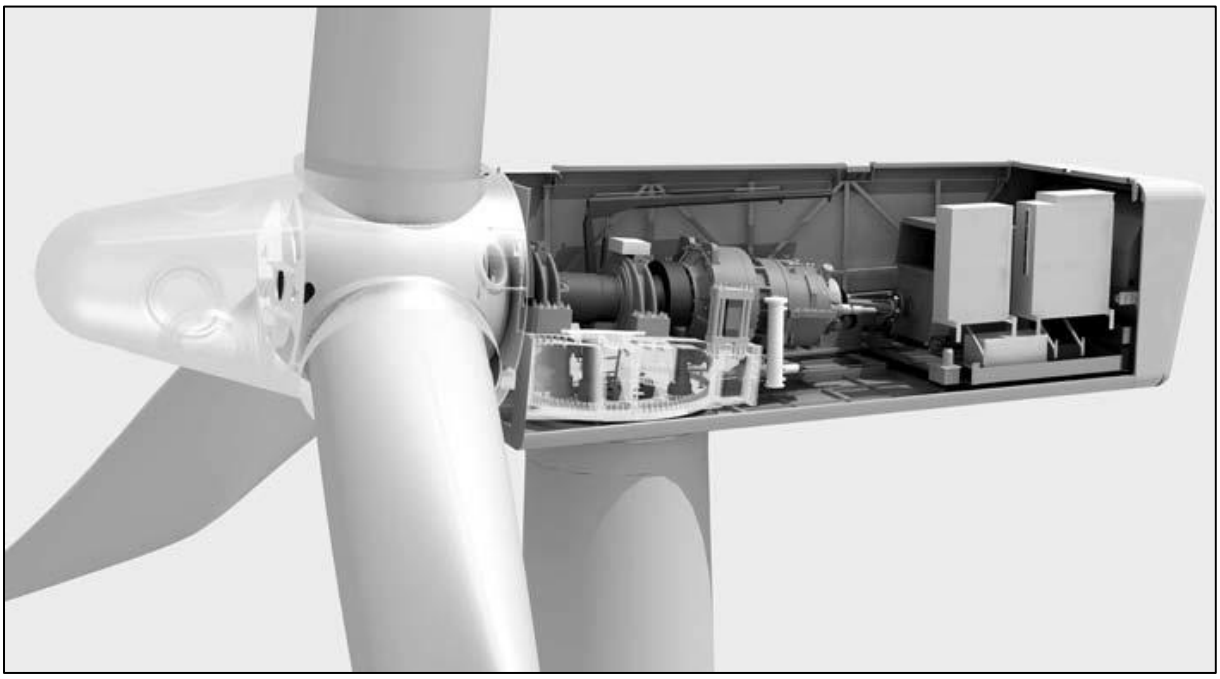

Figure 2.2. Siemens offshore wind turbine [1]

A wind turbine rotor rotates perpendicular to the wind under ideal conditions. Wind turbines generally have a wind vane to determine the direction of the wind. The signal from the vane is coupled with a yaw motor, which continuously turns the nacelle to align its direction with the wind.

In recent years, great developments on the rotor components attract attention. The aerofoils which were developed for aircraft are used on the first modern wind turbine blades but they were not optimized for the much higher angles of attack which occurs frequently on a wind turbine blade. Nowadays, blade manufacturers have focused to use aerofoils specifically optimized for wind turbines. Many different materials have been used in the construction of the blades. They must be strong and stiff, have a high fatigue endurance limit and be as low cost as possible. Most blades are built of glass fibre reinforced plastic today. But other materials such as laminated wood are also used [1].

2.3.Wind Energy in the World

Wind energy is the fastest growing energy type in the world. Figure 2.3 demonstrates the cumulative increase of power in wind energy stations globally between 1996-2009.

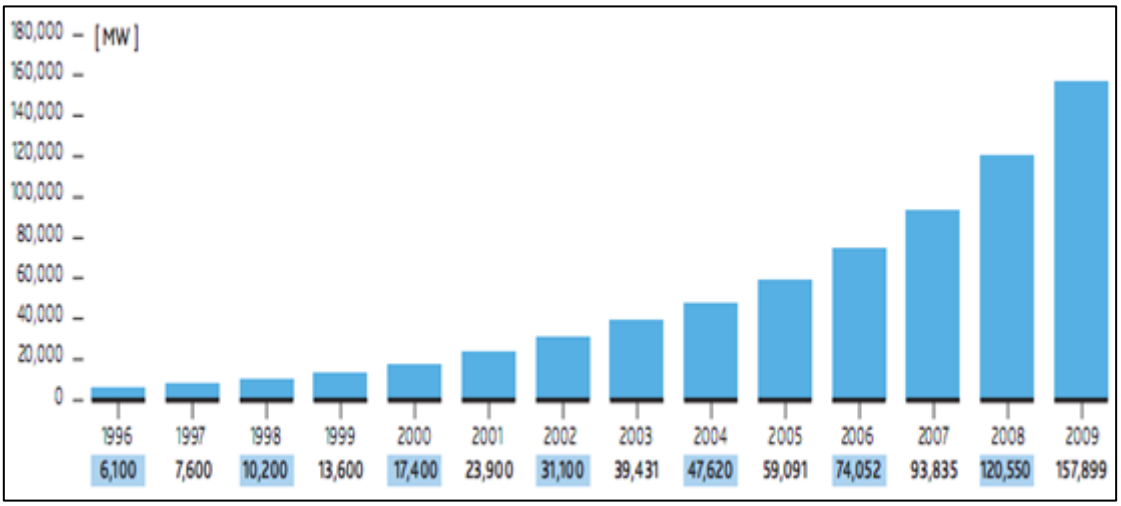

Figure 2.3. Cumulative increase of power [2]

Especially, dramatic increase has been observed after 2005. This does occur only in Europe, but also wind power increase in America, China and India has observed. By the end of 2009, 157899 MW total intalled wind power exists globally. Europe is the leader with 76152 MW. Europe has 48% of the installed wind power in the world. Wind capacity in Europe has increased by 16% which supplies 6% of the electric power need from wind energy. China has also increased its capacity by 110% in 2011 [2].

2.4. Wind Energy in Europe

European Union countries have focused on renewable energy resources especially on wind energy. Usage of wind energy has increased in 2009. Germany is the leader and Spain follows. In Italy and France, usage of wind energy is increasing progressively. By the end of 2008, wind energy power capacity was 65741 MW. In 2009, it increased by 16% and reached to 76152 MW [2].

2.5.Wind Energy in Turkey

In parallel to the global wind power growth installed wind turbine capacity is growing in Turkey. In 2011, 658 MW installed wind turbine capacity was in service while and 402 MW was under construction. Amounts of wind turbines which were operated and under construction according to their power are shown in Figure 2.4.

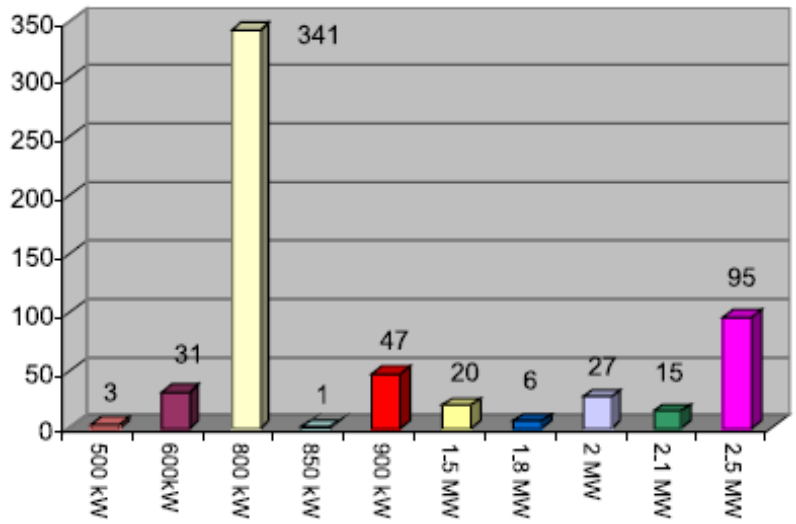

Figure 2.4. Amount of wind turbines according to their power

2.6. Potential of Wind Energy in Turkey

It is important to know specifications of wind resource before planning wind turbine. According to yearly average values, the best places for wind resource in Turkey are coastal areas, high lands and top of mountains at western coast, around Marmara Sea and a small localized area in Antakya. Moderate strength wind resources are also available in Middle Anatolian Region. Figure 2.5 demonstrates wind speed topography in Turkey.

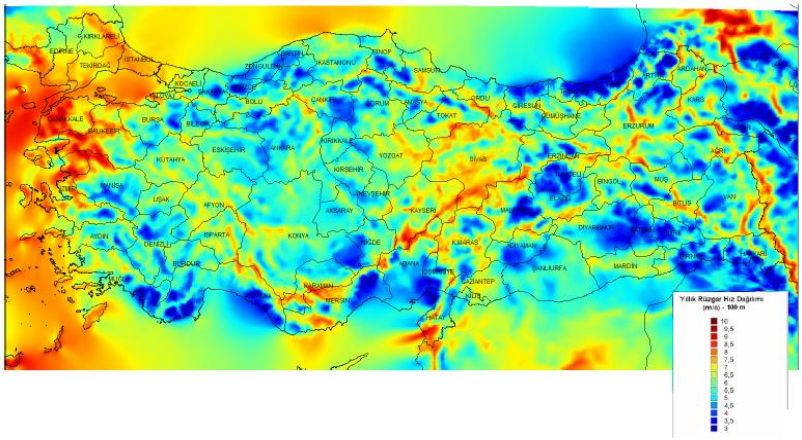

Figure 2.5. Wind Speed Topography in Turkey [4]

2.7. Advantages and Disadvantages of Wind Energy

The most important advantage of the wind energy is that it is a renewable energy resource. It is a green energy which does not have harmful emission and does not pollute environment. Usage of wind energy prevents radioactive waste, air pollution, oil leakage… It creates new employment areas which require skilled workforce and higher education.

There are also some disadvantages. Energy production may change according to unpredictable wind speed. In other words, if wind has not adequate speed, electrical energy might not be produced. There are some ongoing projects to store wind energy for windless days. Another disadvantage is noise. Wind turbines cause approximately 85 dB noise. Therefore, they must be constructed at least 500 m far from settlement areas. Moreover, there are some studies to decrease level of sound. They may also affect radio, television and other communication signals in 3 km diameter [5].

3. BASICS OF WIND ENERGY

During the energy conversions and transactions, air pressure increases and decreases in different regions. This alteration causes air to move from high to low pressure areas. Radiation, vaporization and surface roughness have effects on wind conditions. Effect of pressure difference can be explained with many physics rules. One of them is Boyle Theorem which claims that multiplication of pressure and volume under constant temperature does not change [19].

$$P_1 \times V_1 = P_2 \times V_2 \tag{3.1}$$

Another theorem from Charles which claims that ratio of volume to temperature under constant pressure does not change [18].

$$\frac{V_1}{T_1} = \frac{V_2}{T_2} \tag{3.2}$$

Ideal gas theorem is obtained from these:

$$P.V = n.R.T \tag{3.3}$$

In this theorem, P (Pa) is gas pressure, V (m^3) is volume, n (kmol) is amount of gas molecules, R is universal gas constant and T (°K) is temperature [6].

3.1. Modeling Alterations of Wind Speed

Yearly average of wind speed can be used to predict wind energy on unit area or potential of wind power. It may help to determine places for wind turbine but it does not show yearly changes. Two wind turbines which have same yearly average of wind speed may have different energy potentials. Therefore, hourly averages of wind speed values are used to determine wind energy potentials.

3.2. Determining Potential of Wind Energy

Wind has kinetic energy due to it is a moving air. Kinetic energy equation:

$$E = \frac{1}{2}mv^2 \tag{3.4}$$

In this equation, *E* is energy, *m* is mass and *v* is velocity.

$$m = \rho . v \tag{3.5}$$

$$v = A . L \tag{3.6}$$

A is perpendicular area to wind direction and *L* is length in wind direction. This length equals to distance that gas moves with *v* velocity in *t* time.

$$L = v . t \tag{3.7}$$

When these equations are used in kinetic energy equation (2.4):

$$E = \frac{1}{2}\rho A t v^3 \tag{3.8}$$

To reach energy in unit area and time, *t* and *A* should be taken as 1.

$$E_u = \frac{1}{2}\rho v^3 \tag{3.9}$$

ρ is density of air at the sea level and equals to:

$$\rho = 1.223\ kg/m^3 \tag{3.10}$$

v is wind velocity which is measured at 10 m from sea level [7].

4. WIND TURBINES

Wind turbines can be examined in two groups with respect to their rotation axes such as horizontal and vertical axis turbines.

4.1.Vertical Axis Wind Turbines

The first wind rotors were made as vertical axis centuries ago. However, they are not common as horizontal types. The main reason is that vertical axis rotors cannot use high speed winds efficiently as much as horizontal axis rotors. The first known windmill design is Persian windmill around 1000 B.C. to turn a grindstone. It blocks half of the wind (as shown in the figure) to prevent slowing down by reverse blowing to rotating sails [8].

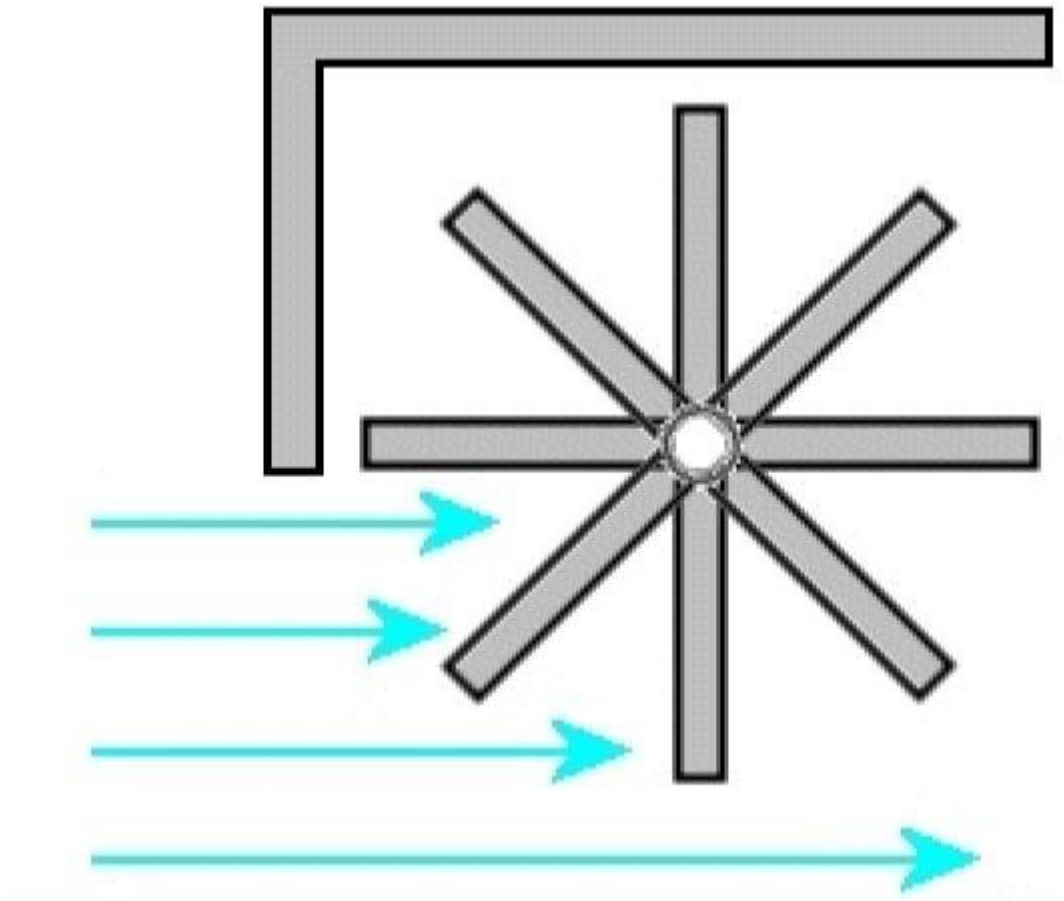

Figure 4.1. Persian Windmill Design [9]

Anemometers are also vertical axis rotors to measure wind speed. Another type of vertical axis rotors is Savonius wind turbines. They have S-shaped sails. It turns relatively slowly, but produces high torque. It is generally used for grinding grain, pumping water and similar local tasks. It is unsuitable to produce electricity on a large-scale due to its low efficiency and slow rotation. Another important wind turbine with vertical axis rotor is Darrieus wind turbine which is the most famous one. It is generally built with two or three C-shaped rotor blades [8]. Their blades are relatively light and turbine is relatively low cost. It is easier to construct and maintain due to its power train, generator and controls are located near ground level. Moreover, the efficiency is nearly competitive with horizontal axis propeller turbine [6].

4.2. Horizontal Axis Wind Turbines

A horizontal axis wind turbine is the most common wind turbine design. In addition to being parallel to the ground, the axis of blade rotation is parallel to the wind flow. It is very common and currently the most efficient system available for wind energy conversion. Figure 4.2 demonstrates components of a horizontal axis wind turbine.

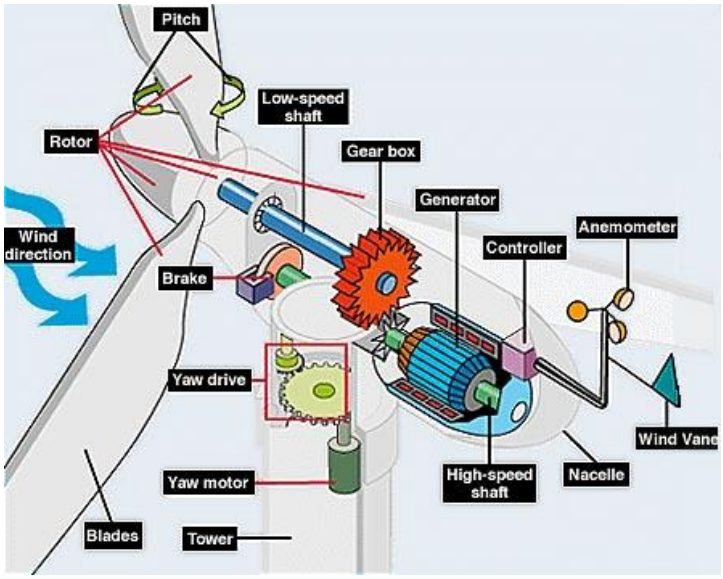

Figure 4.2. Components of the Horizontal Axis Wind Turbine [10]

4.3. Components of the Horizontal Axis Wind Turbine

As it is seen on Figure 4.2, there are many components in a wind turbine. In this thesis, rotor and hub are the focus of the study.

4.3.1. Rotor

Rotor includes blades and hub which blades are connected in wind turbines. It is the most important component with respect to cost and performance. Most industrial turbines are generally upwind turbines with three blades. However, there are also some downwind turbines with two blades. Constant blade angle rotors are used for small and middle scale turbines. However, variable blade angle rotors with control system are used in modern wind turbines. In this study a variable blade angle rotor system has been studied.

4.3.2. Hub

The blades are connected to the hub. This component transmits the power which is taken from blades to the generator via a transmission shaft. Design and manufacturing of the hub component is crucial as it is exposed to many different critical loads. Casting is generally preferred for fatigue loading [11].

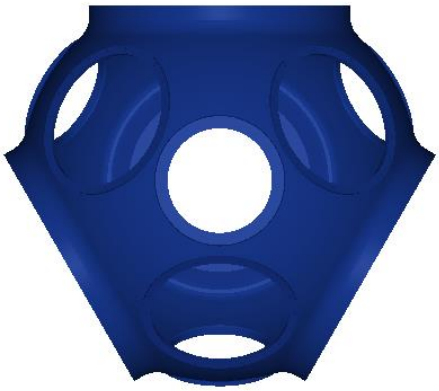

Figure 4.3. Hub

5. DESIGN OF THE HUB AND FINITE ELEMENT ANALYSIS

In this study, structural finite element analyses have been conducted for wind turbine hub with the loads acting on the connecting slew bearings between blades and hub. 3D design has been created in SolidWorks, and HyperMesh has been used to obtain finite element model. Finally structural analyses have been performed using ABAQUS. Some physical data from the analysis conditions are given in Table 5.1.

	Symbol	Unit	Value
Turbine Power	P	kW	500
Rotor Diameter	D	mm	46000
Rotor Cycle	n	rpm	22.4
Rotor Angular Speed	φ	rad/s	2.3
Mass of Hub	m_H	kg	2980
Hub Diameter	d	mm	1900

Table 5.1. Physical Data for Wind Turbine

Elastic movements of blades and reactions due to elastic behavior have not been included to these analyses. Rotor and blades have been accepted as rigid body. Pre-design mass information has been used for blades.

Aerodynamic loads have been defined on y-z plane and x as outer axis as it is illustrated in Figure 5.1. This figure has been created for the first blade and it rotates with angular speed of the rotor. Wind direction is negative x axis. Loads have been calculated

at the connecting slew rings at bottom points of the blades. The moment which bends the blade out of the plane (around positive y) is called as outer plane moment (M_y). The moment that bends the blade in plane (around positive x) is called as inner plane moment (M_x). The moment that bends blade around radial axis (around positive z) is called as torsional moment (M_z). The force that acts through outer plane (negative x direction) is called as outer plane cutting force (F_t). The force that acts in inner plane (negative y direction) is called as inner plane cutting force (F_y). Rotation of the blade around negative z axis is called as positive pitching. Table 5.2 presents the data that is used to determine wind turbine class.

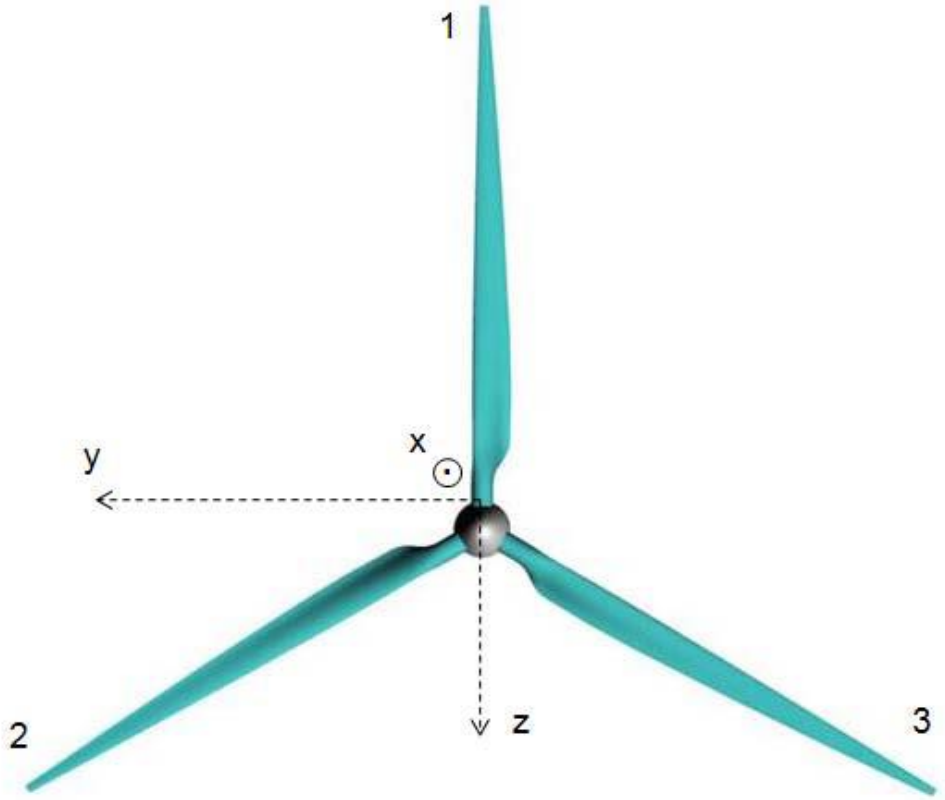

Figure 5.1. Axes for Aerodynamic Loading Definition

Average wind speed	m/s	6.5
Extreme wind speed	m/s	60
Tower Height	m	65
Rotor Rotation Speed	rpm	28
Rotor Hub Diameter	m	2

Table 5.2. Information about Wind and Turbine

Wind conditions and related loads have been examined for all pitching angles from -16 to +32 with 4 degrees intervals. Analysis scenarios have been chosen from these load combinations by selecting the maximum loading effects. Two worst scenarios are denoted in Table 5.3. It should be noted that these extreme pitch angles only happen in rare unusual conditions. Typical operating pitch angles occur between 0 to 16 degrees interval.

	M_y (kNm)	M_x (kNm)	M_z (kNm)	F_t (kN)	F_y (kN)
1.Scenario Blade Angle = 32	643.6	515.6	-5.3	60.3	12.4
2.Scenario Blade Angle = -8	1290	285	-1.9	98.9	18

Table 5.3. Loading Conditions for Analyses

Abbreviation	Definition
My	Outer plane moment
Mx	Inner plane moment
Mz	Torsional Moment
Ft	Outer plane cutting force
Fy	Inner plane cutting force

Table 5.4. Definitions of abbreviations

5.1.Material Information

Hub has been modeled with shaft, bearings, bolts and nuts to simulate the environment as realistic as possible. Therefore, material information of each component has been found and added to the model. Hub is designed with ENGJS-400-18-LT casting material. This material has more elongation ratio than other casting materials. Bolts and nuts are selected as Class 12.9. Bearings are manufactured by specifically with respect to boundary conditions and loads. Mechanical properties of each component are given in Table 5.5.

	Hub (ENGJS-400-18-LT)	Shaft	Bolts and Nuts (Class 12.9)	Bearings
Elastic Modulus $[N/mm^2]$	1.2×10^8	1.2×10^8	2.05×10^8	2.1×10^8
Density $[kg/m^3]$	7250	7250	7850	7830
Poisson's Ratio	0.26	0.26	0.29	0.28
Yield Strength $[MPa]$	250	685	1100	310
Tensile Strength $[MPa]$	400		1250	

Table 5.5. Mechanical Properties of Materials

5.2. Mesh Process

Finite element model has been created via HyperMesh. This software allows usage of flexible and user-defined elements. Therefore, more realistic and accurate results can be obtained for each part of the model. Moreover, it minimizes finite element errors which are caused by inadequate modeling.

First, 3D design has been obtained in SolidWorks. Since, wind turbine has many different components, due to intricate connections each component has many detail features on their bodies. Most of the details and structurally unimportant features have been omitted in engineering simulations. After the simplifications, HyperMesh software has been used to create 2D surface elements. Especially, bolts and locations around bolt holes are very important areas because of the heavy loads acting on such areas. Therefore, these areas have been meshed carefully and in detail. Tria elements on flat surfaces and R-tria elements on circular surfaces have been utilized. The detail mesh can be seen around the bolts, bolt holes and corner points in Figure 5.2. These surface elements can be used to generate a tetrahedral mesh later on.

After the model surfaces have been meshed by 2D elements, 3D tetramesh elements (Figure 5.3) have been created based on the 2D surface elements. This method allows an

engineer to control every detail of the model to simulate the system in more accurate and realistic way.

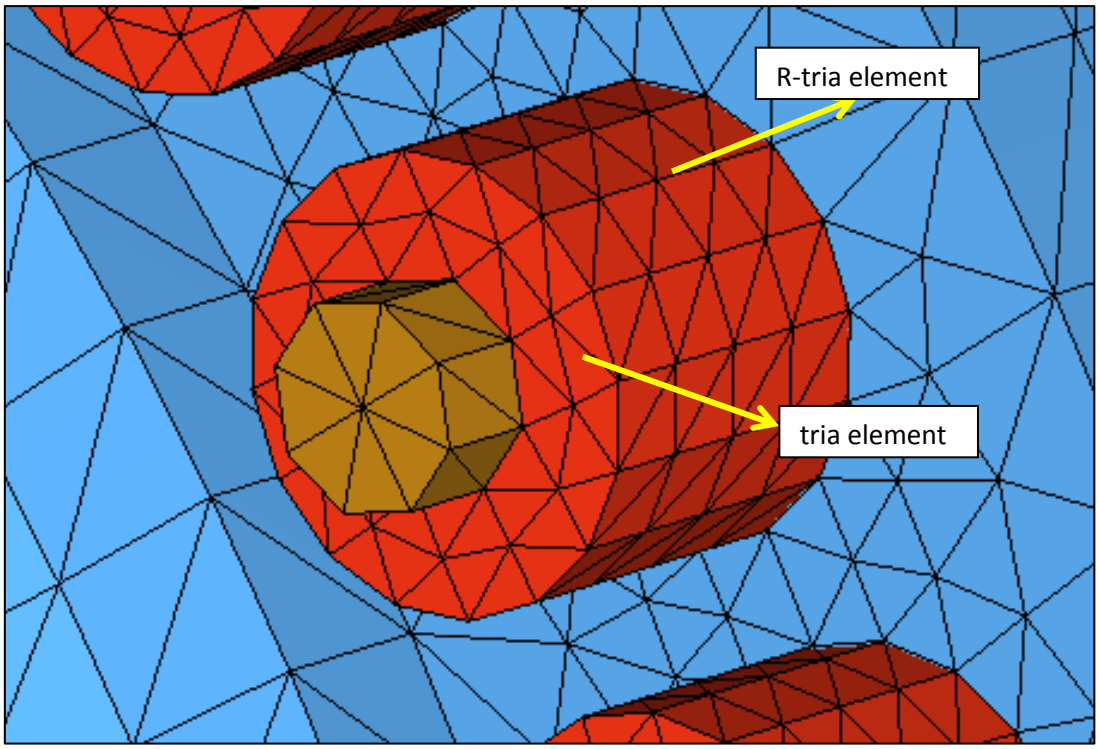

Figure 5.2. Tria and R-tria elements

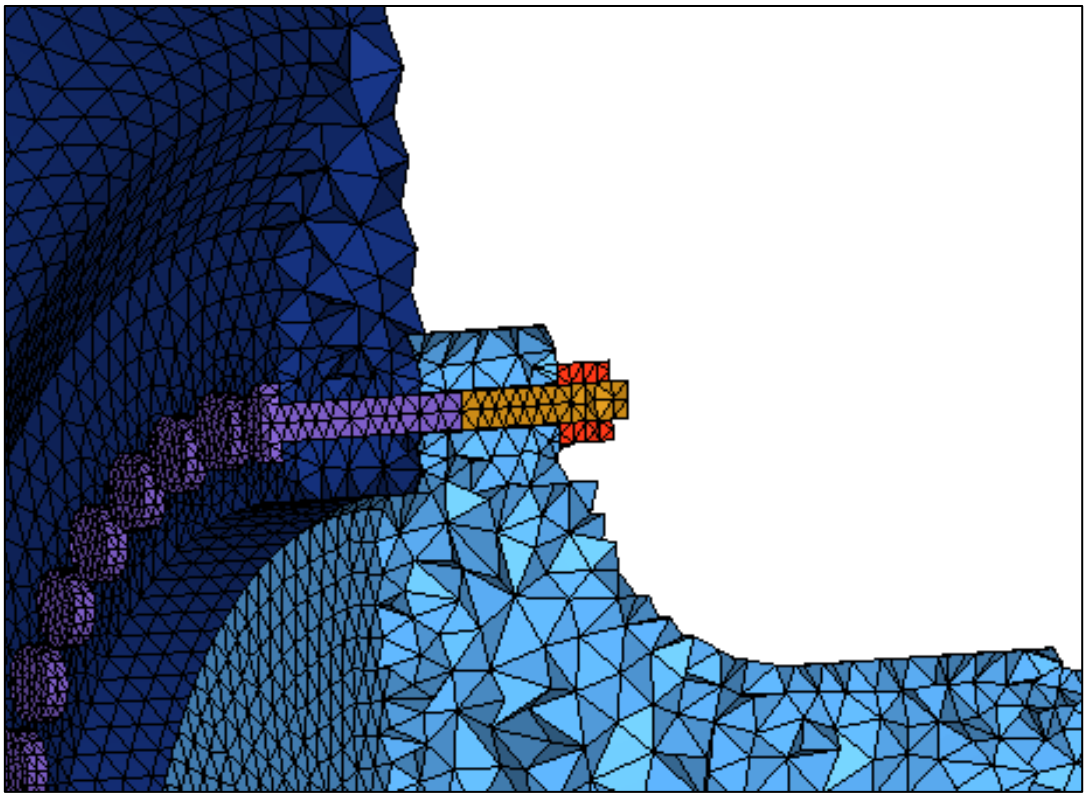

Figure 5.3. A cut view from the generated tetramesh.

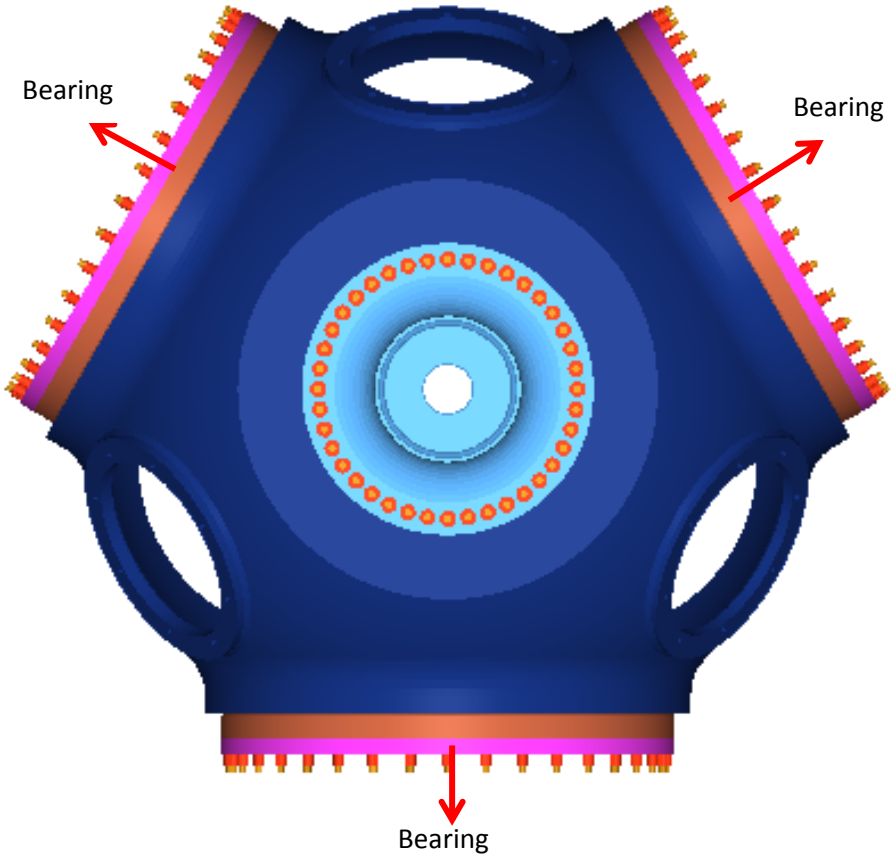

Figure 5.4. Wind Turbine Rotor – Front View

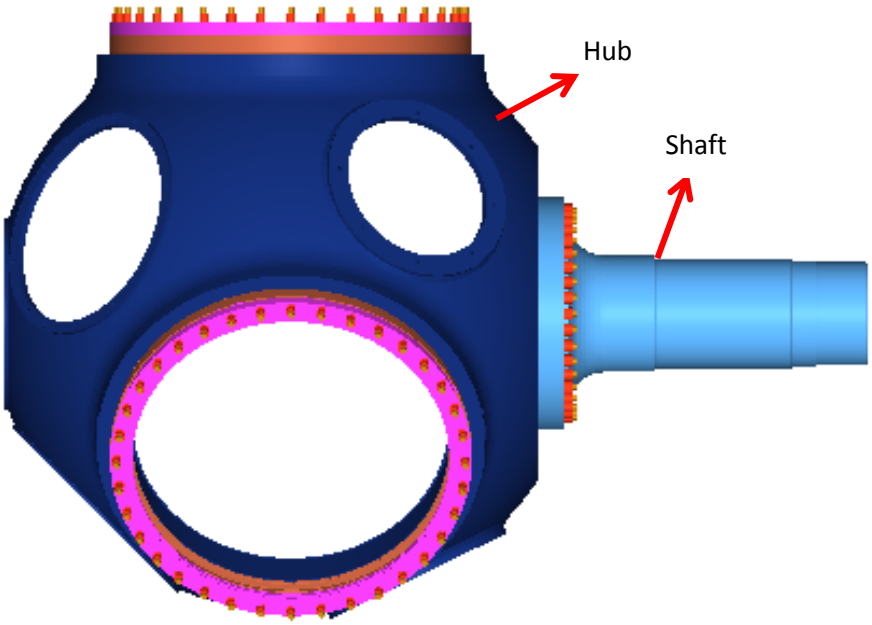

Figure 5.5. Wind Turbine Rotor – Side View

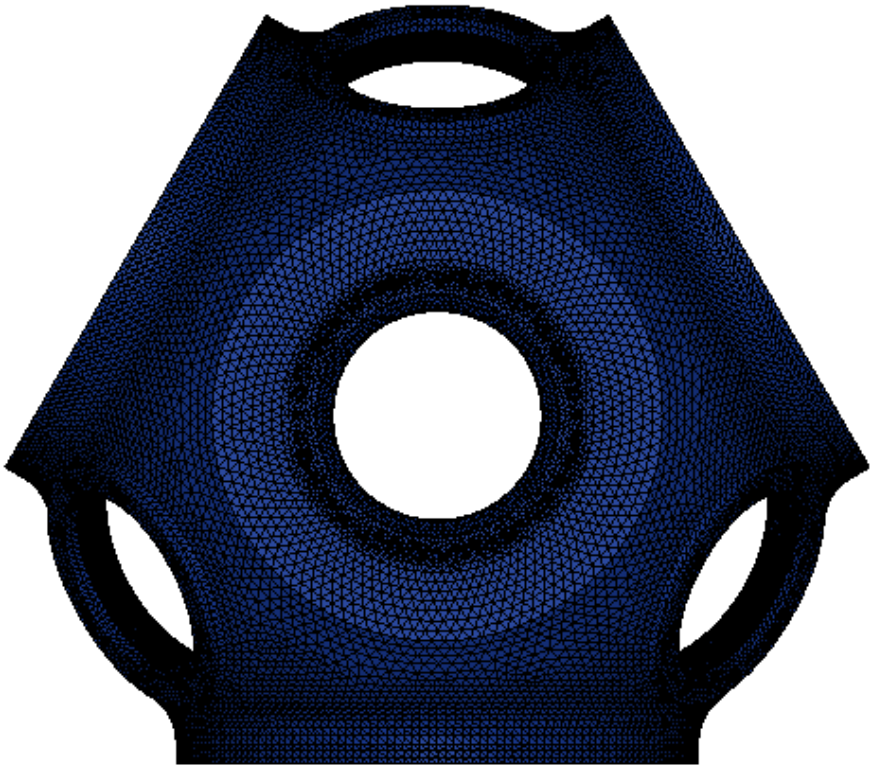

Figure 5.6. 3D Mesh on Hub

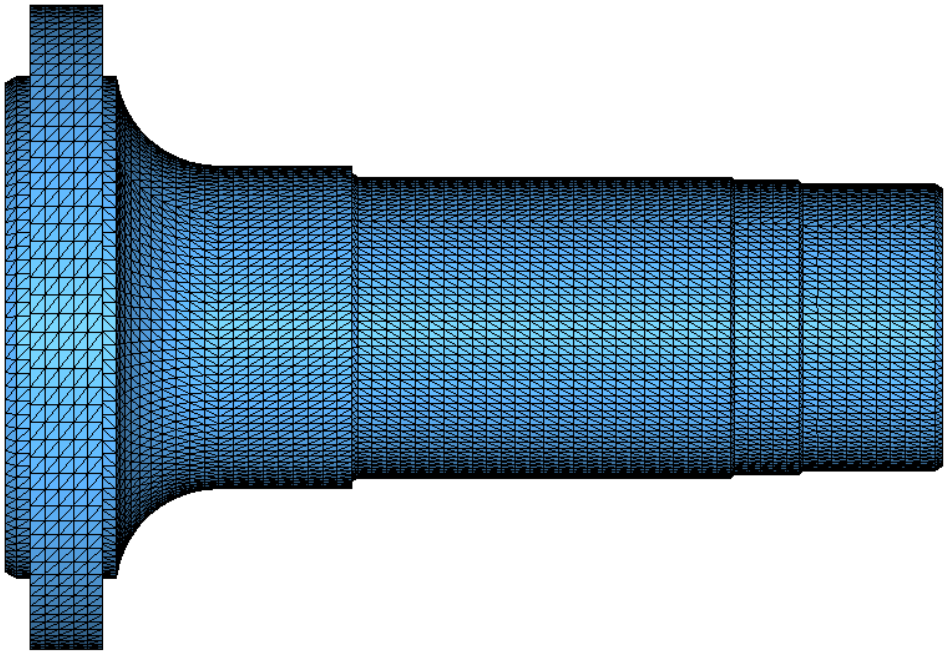

Figure 5.7. 3D Mesh on Shaft

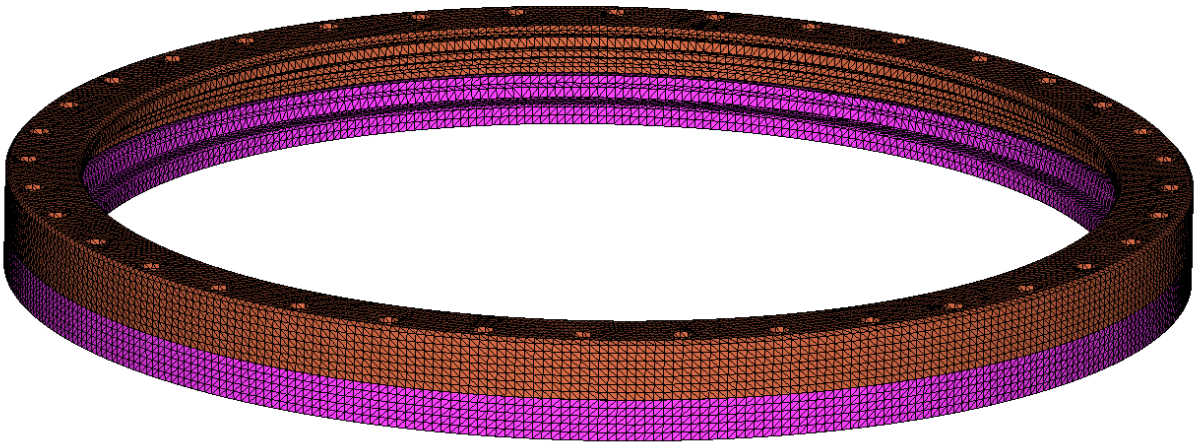

Figure 5.8. 3D Mesh on Bearing

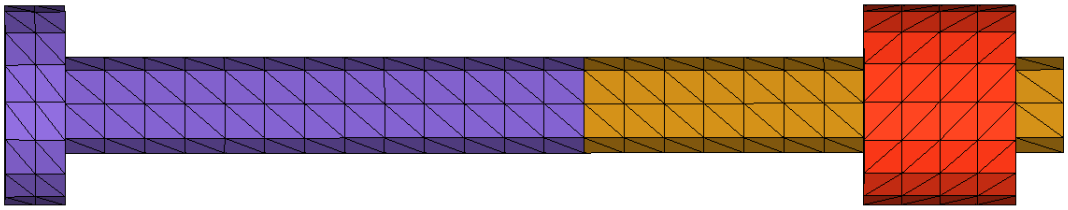

Figure 5.9. 3D Mesh on Bolt and Nut

To ensure quality of the finite element analyses, a quick mesh sensitivity study has been conducted. After a few iterations, the mesh has been refined. The final mesh includes 2,400,013 nodes and 1,414,003 elements. A fine mesh has been generated especially at bolts, nuts and around bolt holes. These parts and areas are exposed very high loads. Many subcomponents have been simplified as much as possible. For example, the slew ring bearings that connect blades to hub have two parts. One side is connected to blades while other half is bolted to the hub. The part of the slew rings that are bolted to the blades have been removed from the model for simplification. The loads have been calculated at bottom of the blades have been applied via RBE3 elements and carried over to the hub from the bottom parts of the bearings. After all these simplifications, typical structural FE analysis took about 10 hours to converge with the refined mesh on Xenon processor with 256 GB RAM.

There are 148 bolts and 296 nuts which are M24 Grade 12.9. 40 of them have been used in hub-shaft connection. In addition, washers have been modeled for head and nut sides of the bolts that connect shaft to hub.

5.3.Modeling Process

After the meshing process is completed in HyperMesh, finite element analyses have been performed in ABAQUS software. This process has been completed in four steps.

5.3.1. Contact Modeling

In this step, contacts have been defined. The contact modeling has been conducted standard hard contacts. All component-to-component contacts, such as bolts, nuts and part interfaces have been included in contact definition process. An average standard friction coefficient of 0.4 has been applied for every contact.

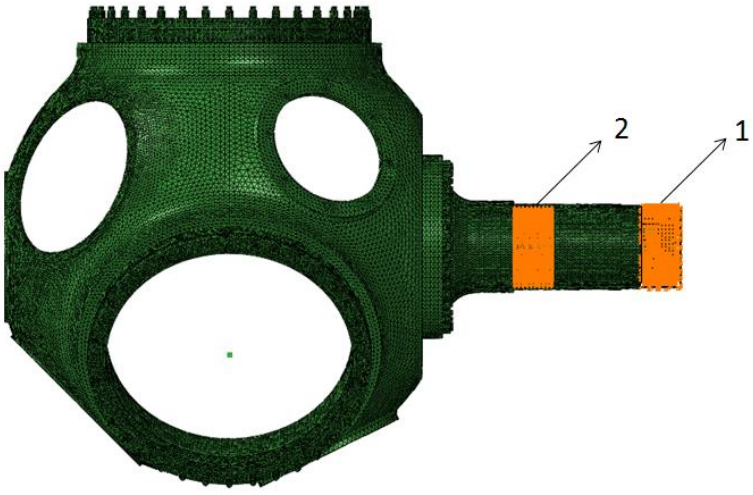

Figure 5.10. Model Fixation

5.3.2. Bolt Preloads

Bolt loads are added to model in this step. 307723 N bolt-load which is equal to 90% of proof load is applied as preload for each bolt. Bolts are modeled with two parts. Bolt load is defined on mid-surface between these parts. Solver pulls both parts towards the middle per preload amount. Bolts do not have any contact with their holes. Software defined bolt-nut connection type is applied in these analyses.

5.3.3. Gravity Loads

Mechanical properties of the materials have been defined in HyperMesh model. Model has been created based on the real 3D design. Therefore, gravitational force is calculated by multiplication of density and volume and added in positive z direction with respect to Figure 5.1. It is important to observe openings and stress values at hub-shaft connection.

5.3.4. Force and Moment Loads

To allow any load application on the model, the mesh has been fixed at two different locations. Actual rotor assembly is supported at two bearings. The upwind bearing is the main bearing is labeled as #2. This bearing is modeled to support radial loads only. The down wind bearing is labeled as #1. This bearing is modeled to support both radial and axial thrust loads. Therefore, as illustrated in Figure 5.10, the model has been supported at area #1 from all directions, and at area #2 from radial direction. By holding the rotor in all directions at bearing #1, it is assumed that the torque transfer to the rest of the system occurs at this location.

All aerodynamic forces, moments and centrifugal forces are applied in this step. These loads that are presented in Table 5.3 are the main loads in this analysis. A radial coordinate system has been created at the bottom of each blade. Loads are applied with

respect to these coordinate systems to blades. Therefore, loads are carried over to whole system by RBE3 elements which have been located at the bottom of blades.

5.4. Analysis Results

Two different working scenarios with different blade angles have been chosen and analyzed.

5.4.1. The First Scenario

The first analysis scenario represents a very high pitch angle case where blade angle is 32 degrees. Typically, wind turbines operate between 0 to 16 degrees pitch angle. The corresponding load levels are presented at Table 5.3 for this case.

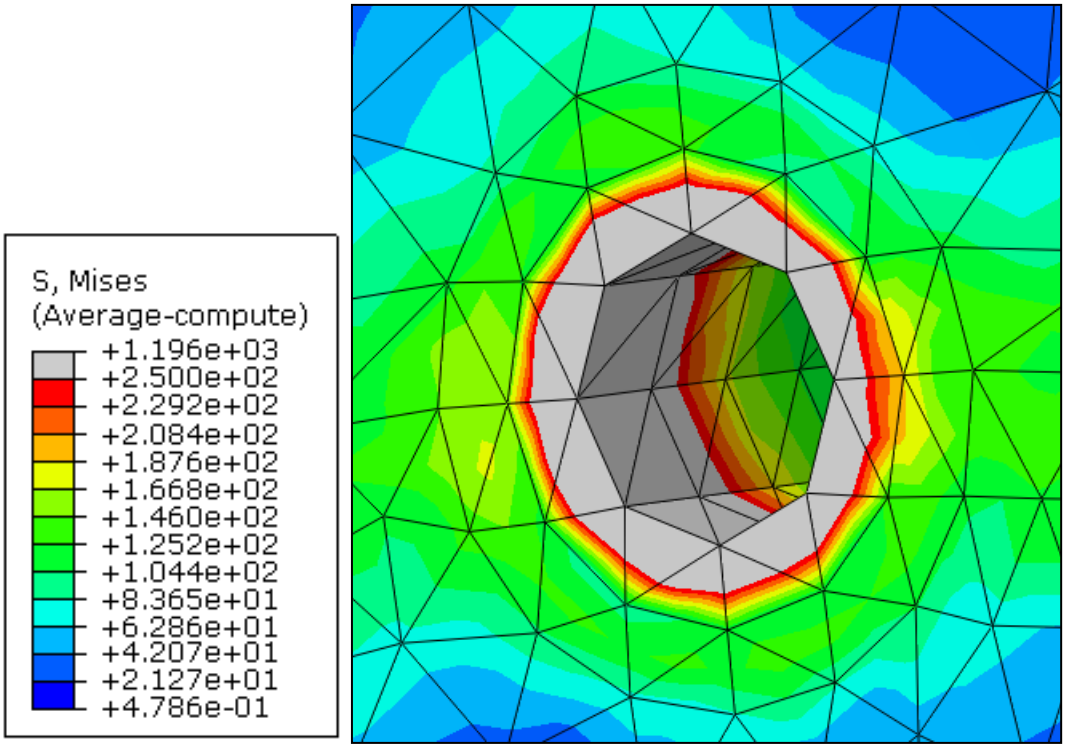

Figure 5.11. Bolt Hole Analysis Results – Scenario #1

The analysis results indicate some local high spots near the bolt hole edges. This behavior is expected finite element singularity near sharp edges. Typically, the values at the neighboring nodes are used in such cases. Figure 5.11 illustrates local stress concentration near a bolt hole. Other than these localized stress concentrations there are some high stress areas near the man holes on hub component. However, these values do not exceed the yield strength (250 MPa) of the material. Therefore, even under such an extreme loading situation hub can be accepted as safe for this scenario. Detailed illustration is demonstrated in Figure 5.12.

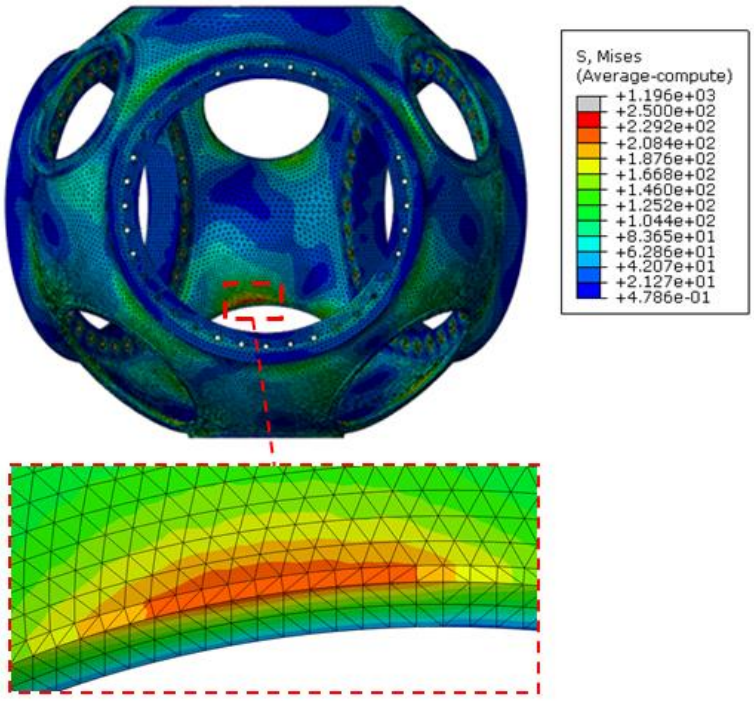

Figure 5.12. Hub General Analysis Results – Scenario #1

As for the bolts, the stress values are generally below the yield strength (1100 MPa). However, there are some local high spots at the bolt head edges with high stress values due to finite element singularity issues. Detailed results are shown in Figure 5.13.

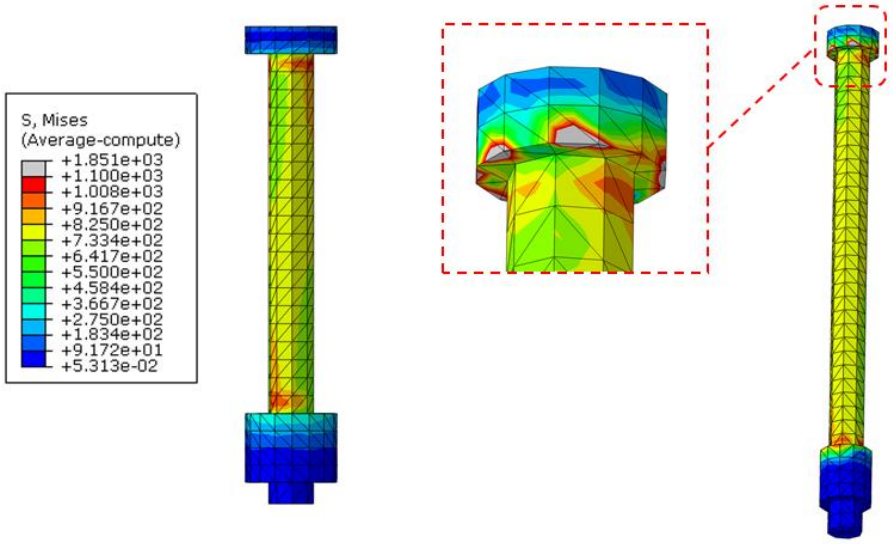

Figure 5.13. Bolts and Nuts Analysis Results – Scenario #1

Stress in the shaft component is below the yield strength (685 MPa). There are some local high points near a fillet around bearing #1. These high spots appear due to discrete and simplified modeling of the small fillet. It is demonstrated in Figure 5.14.

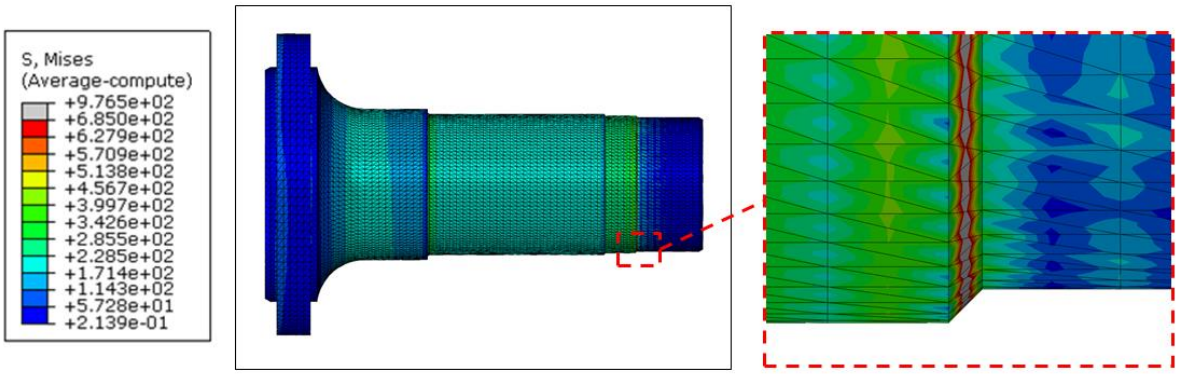

Figure 5.14. Shaft Analysis Results – Scenario #1

When deflections are examined, it appears that hub deflection at the front end is maximum due to its own weight. Figure 5.15 shows that maximum displacement is around 2 mm.

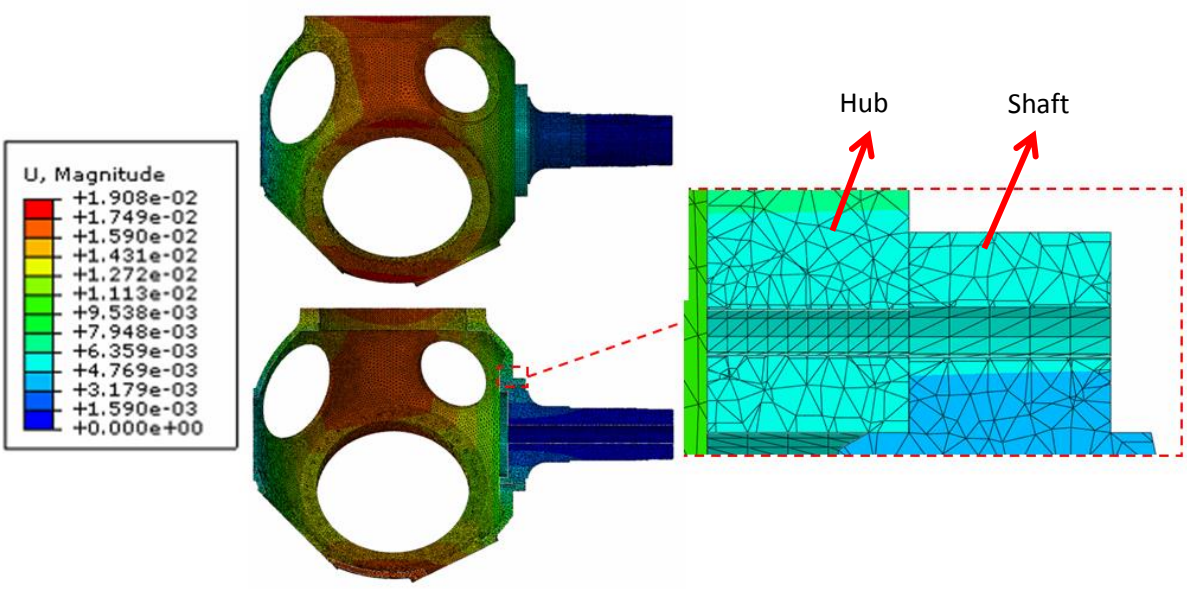

Figure 5.15. Displacements – Scenario #1

The hub-shaft contact has been examined to check if the bolt preload is safe and there is no relative motion at this contact. The results indicate that this contact is in sticking status. In other words, these parts are not moving relative to each other. Therefore, bolt load and friction force is sufficient to prevent any slip between hub and shaft. CSTATUS module of ABAQUS helps us to understand these issues easily as in Figure 5.16.

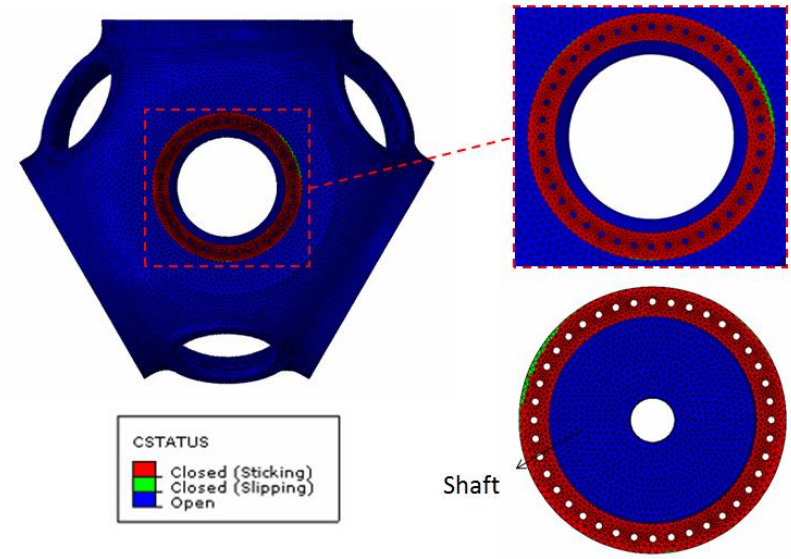

Figure 5.16. Hub-Shaft Connection Contact Status – Scenario #1

Contact pressure values between hub and shaft are adequately high. Therefore, it can be accepted that there is no openings between these two components and there is no slip. Contact pressure values have been given as MPa in Figure 5.17.

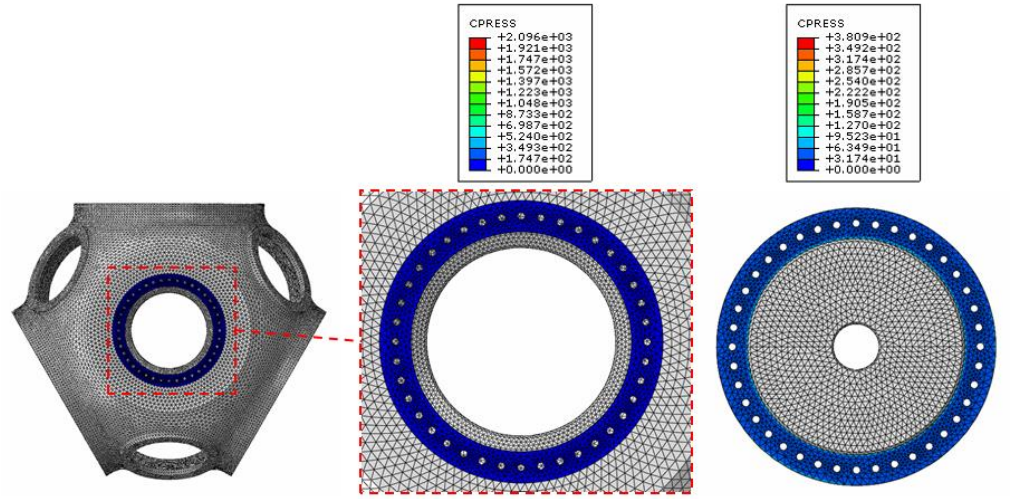

Figure 5.17. Hub-Shaft Contact Pressure – Scenario #1

COPEN (Contact Opening) module of ABAQUS gives the opening value in contact areas. It is about zero at hub-shaft contact as illustrated in Figure 5.18. Opening values are given as mm.

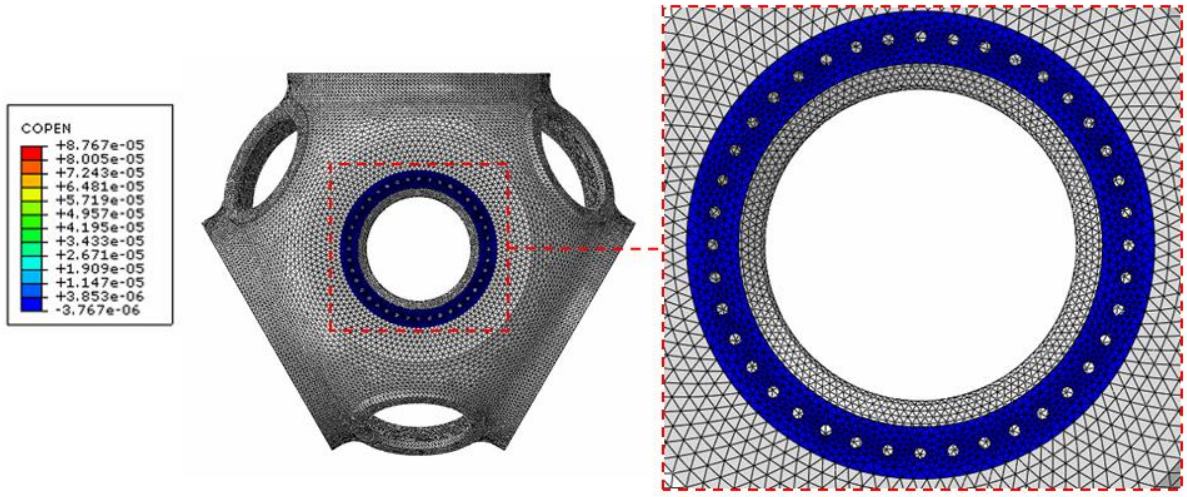

Figure 5.18. Hub-Shaft Contact Opening – Scenario #1

5.4.2. The Second Scenario

The second analysis scenario is a case where blade angle is -8 degrees. This case does not happen in regular operating. Very small negative pitch angles may occur during an emergency brake condition that may be experienced only once or twice in a life time of the equipment. However, this case has been evaluated as a what-if scenario. The corresponding load levels are presented at Table 5.3 for this case.

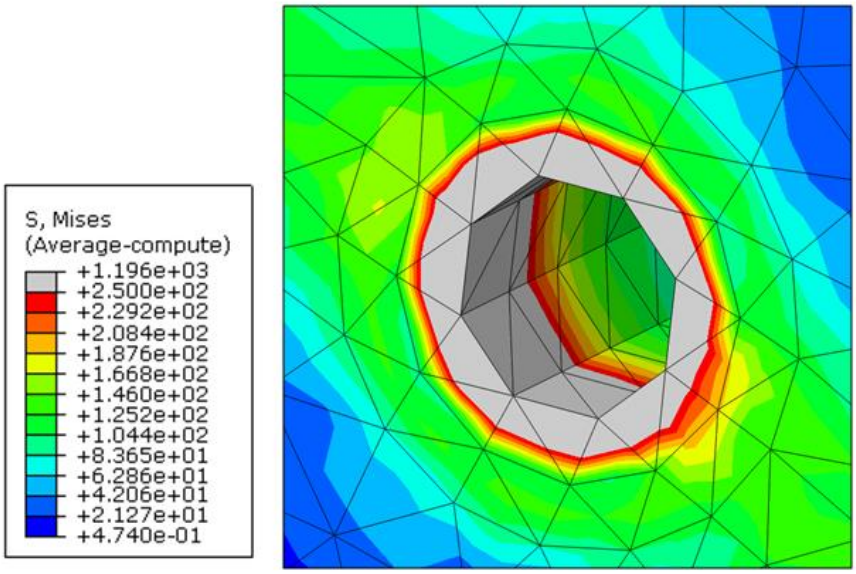

Figure 5.19. Bolt Hole Analysis Results – Scenario #2

The analysis results indicate some local high spots near the bolt hole edges. This behavior is expected finite element singularity near sharp edges. Typically, the values at the neighboring nodes are used in such cases. Figure 5.19 illustrates local stress concentration near a bolt hole.

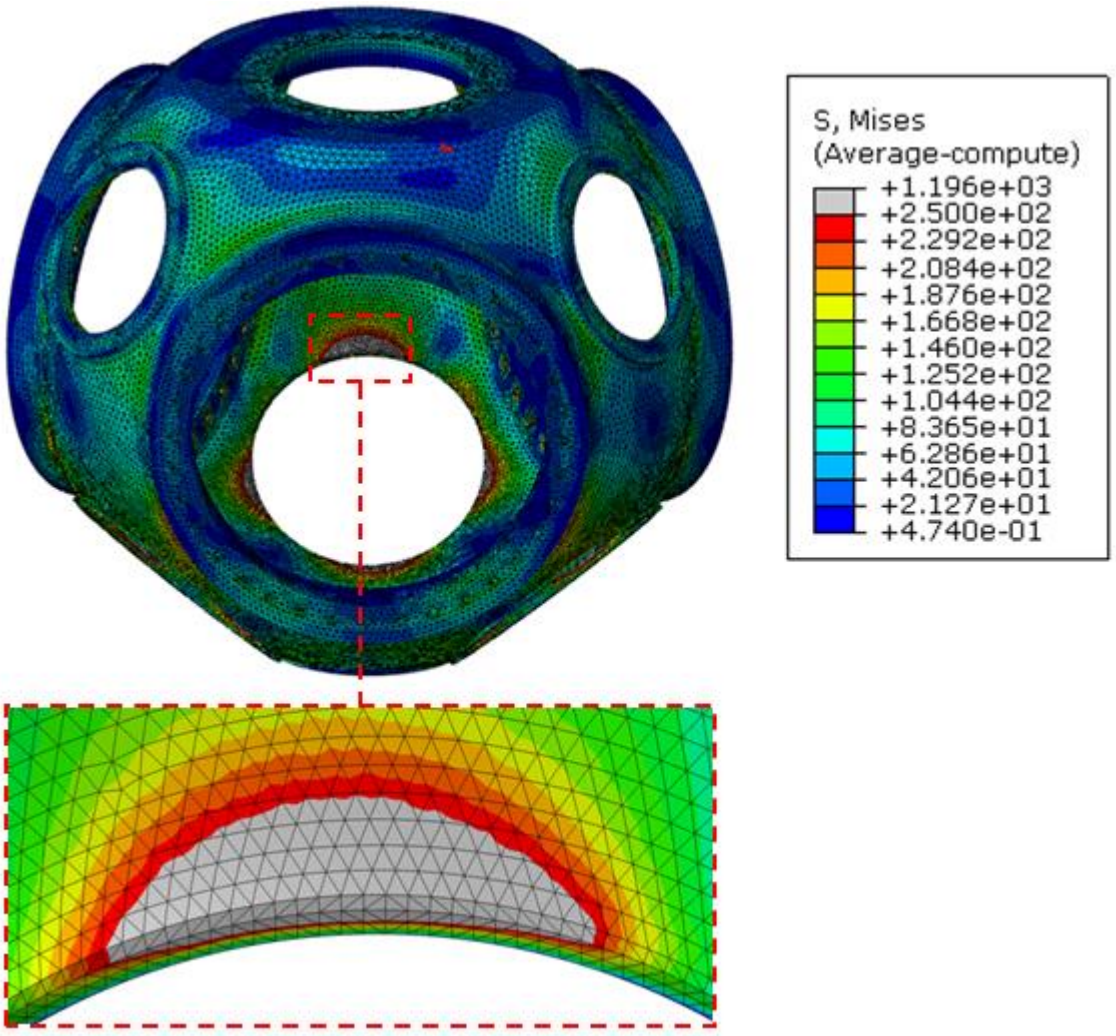

Figure 5.20. Hub General Analysis Results – Scenario #2

Other than the localized stress concentrations and singularities near the bolt hole edges, there are some high stress areas around the weight reduction holes in the hub component. At some points around these holes, high stress levels that exceed the yield strength (250 MPa) of the material can be observed beyond the edge nodes that may experience finite element singularity. The high stress regions extend well beyond edge nodes indicating that this loading may cause a yield failure this area. Therefore, under this unlikely loading scenario local plastic deformation may occur. Detailed illustration is demonstrated in Figure 5.20. It should be noted that, under these extreme loads (per 60 m/s once in 50 gust level) turbine is kept at park not in operation.

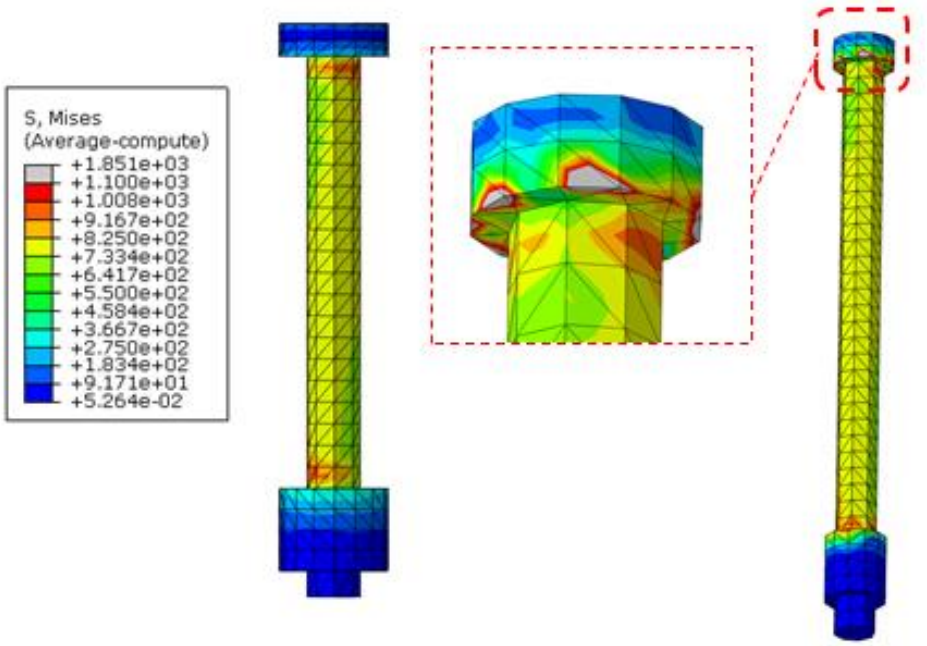

Figure 5.21. Bolts and Nuts Analysis Results – Scenario #2

As for the bolts, the stress values are generally below the yield strength (1100 MPa). However, there are some local high spots at the bolt head edges with high stress values due to finite element singularity issues. These areas are local and there are large differences with their neighbor areas. Detailed results are shown in Figure 5.21.

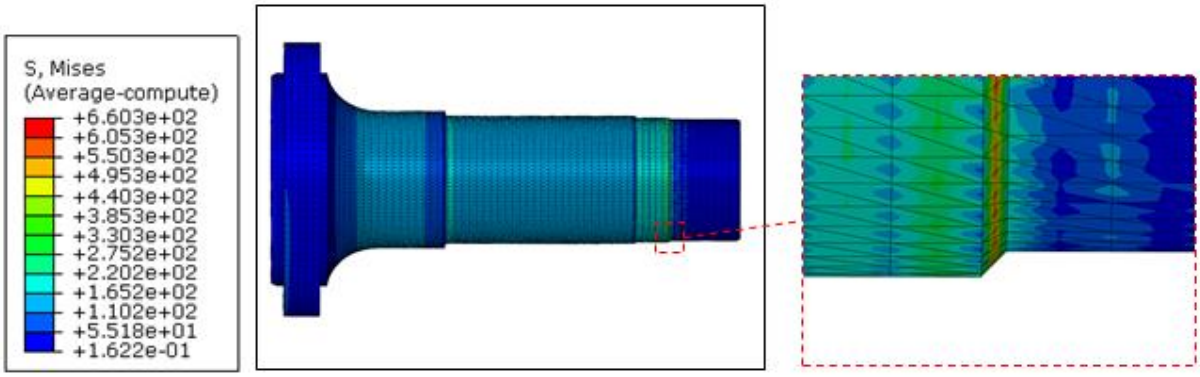

Figure 5.22. Shaft Analysis Results – Scenario #2

Stress levels for all regions of the shaft component are below the yield strength (685 MPa). The highest stress values are observed at the fillet location near bearing #1 as in the first scenario, but they do not exceed the yield strength. It is demonstrated in Figure 5.22.

When deflections are examined, it appears that hub deflection at the front end is maximum due to its own weight. Figure 5.23 shows that maximum displacement is around 1.2 mm.

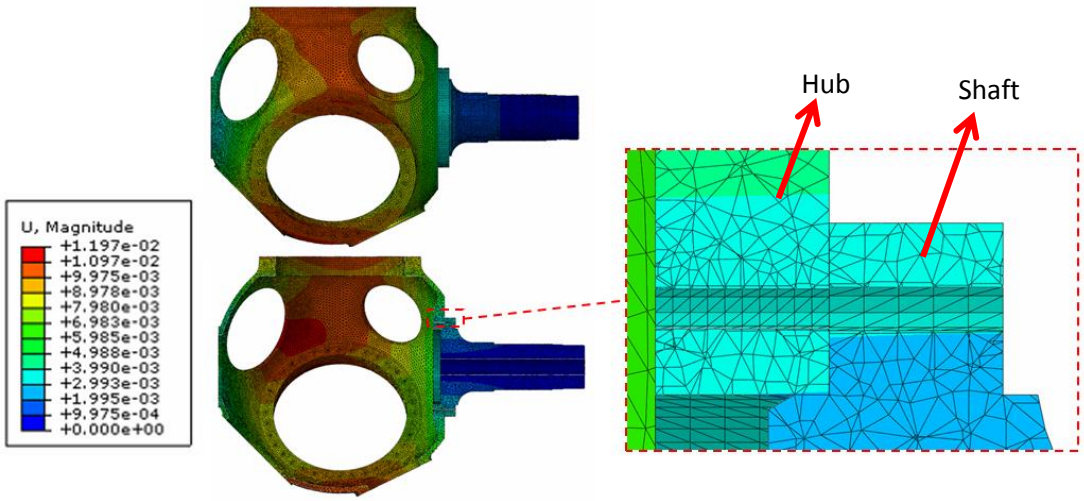

Figure 5.23. Relative movement of hub and shaft – Scenario #2

The hub-shaft contact has been examined to check if the bolt preload is safe, and there is no relative motion at this contact. The results indicate that this contact is in sticking status. In other words, these parts are not moving relative to each other. Therefore, bolt load and friction force is sufficient to prevent any slip between hub and shaft. CSTATUS module of ABAQUS helps us to understand these issues easily as in Figure 5.24.

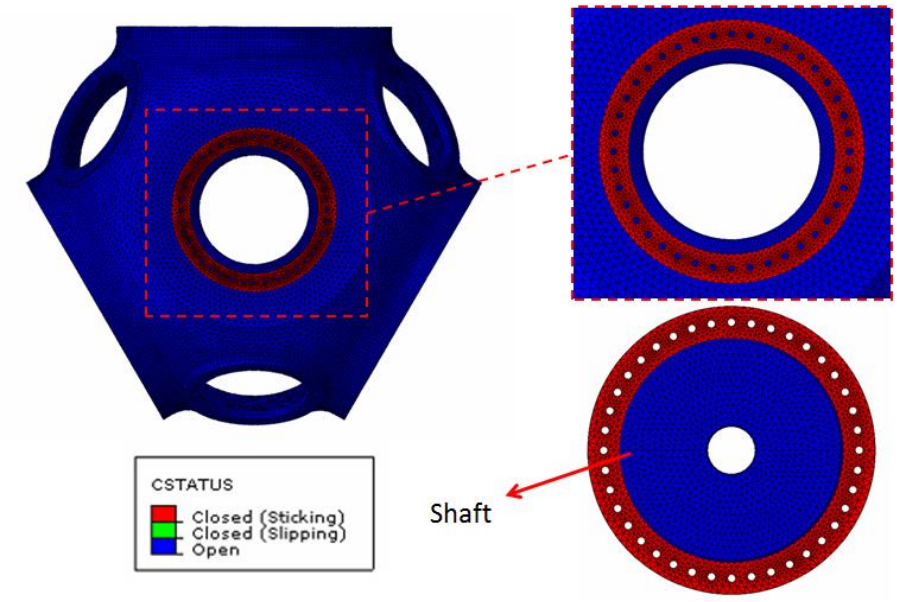

Figure 5.24. Hub-Shaft Connection Contact Status – Scenario #2

Contact pressure values between hub and shaft are adequately high. Therefore, it can be accepted that there is no slip between these two components. Contact pressure values have been given as MPa in Figure 5.25.

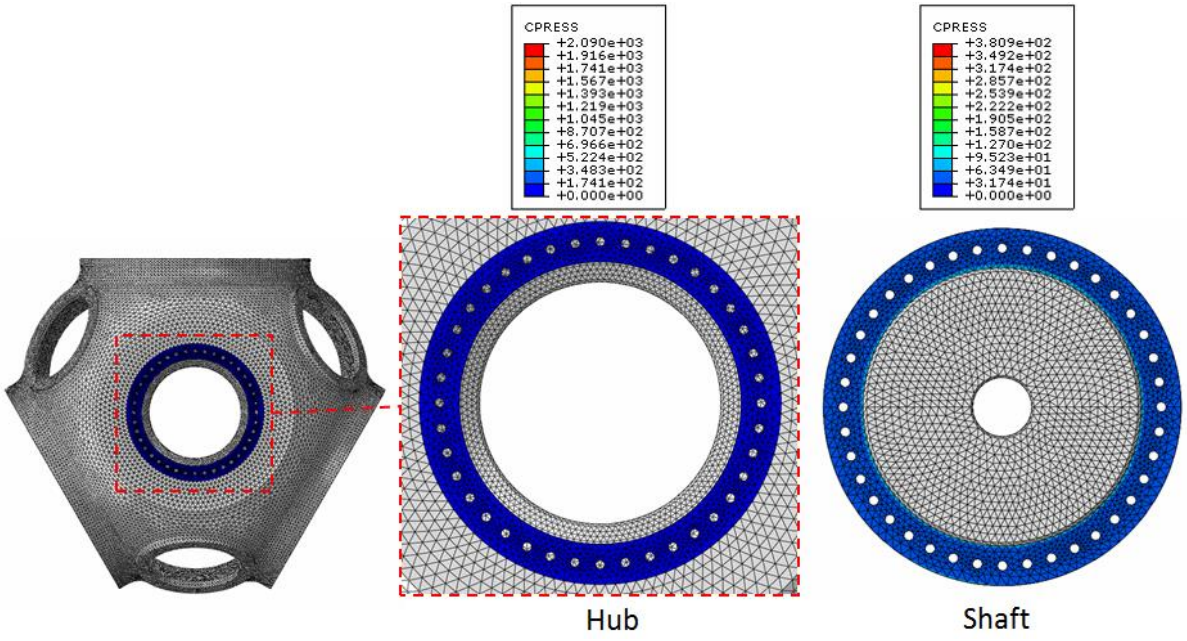

Figure 5.25. Hub-Shaft Contact Pressure – Scenario #2

Opening values are around zero at hub-shaft contact as in Figure 5.26. Opening values are given as mm.

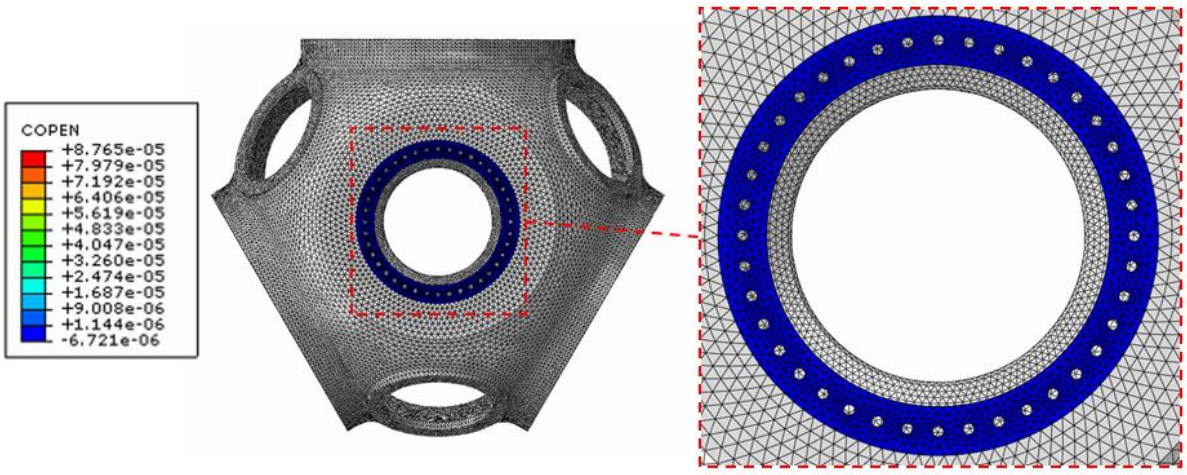

Figure 5.26. Hub-Shaft Contact Opening – Scenario #2

5.4.3. Structural Analysis Summary

ANALYSES SUMMARY						
	Stress			Slip		
	Hub Yield = 250 MPa	Bolt and Nut Proof = 970 MPa	Shaft Yield= 685 MPa	Hub-Shaft [mm]	Hub-Bolt [mm]	Shaft-Bolt [mm]
Scenario #1 (Blade angle = 32°)	200 - 210	830 - 900	300 - 350	0.000031979	0.000007848	0.000016865
Scenario #2 (Blade Angle= -8°)	340 - 350	820 - 870	250 - 300	0.000026586	0.000003732	0.000002603

Table 5.6. Analyses Summary

Structural analysis results are summarized in Table 5.6. Stress values are generally below the material yield strength values. However, in the second load case scenario with -8 degree blade pitch angle, hub component has excessive stress values around weigh reduction holes.

All contacts are safe with adequate bolt loads. Very low slip values indicated in Table 5.6 are within numerical error range in finite element calculations indicating practically zero.

6. FATIGUE ANALYSIS

6.1. Metal Fatigue

Effect of changing load conditions may be ignored at the times when use of metal structures started, because the varying stress levels were so low with respect to main static loads. However, scientists later discovered that alternating load conditions have much more effect than static situations. Rankine had defined some characteristic specifications of fatigue ruptures. Fairbaim made some tests about fatigue ruptures. Lastly, Wohler had published a book which claims that changes in load forms is important as alternating loads. In those years, it was discovered that metal structures may be damaged under low loads with changing conditions [13].

Fatigue is defined as damage of the material under dynamic loading. Machine parts generally work under alternating loads and stresses. Although most loads are static, operating conditions may cause these unsteady loads and stresses. Damage which is caused by this type of conditions is called as fatigue rupture. Beginning point of these damages is caused by singularities and discontinuous structure of materials [17]. These may lead to damage or rupture even static loads are in safe region [15].

6.2. Causes of Fatigue Fracture

Common causes of fatigue fracture can be stated as follows:

- There are high stress values at notch regions.
- Crystal structures at surface are less stiff than inner regions. Therefore, fracture risk is higher at these regions.
- Some atmospheric reactions are effective [13].

Fatigue fractures generally occur at regions where stress intensity is high due to sharp section change or another effect which changes stress intensity [16]. These reasons decrease material life. Any kind of discontinuity may be a reason to increase local stress values [13].

6.3. Fatigue Analysis of the Hub

In this work, a commercially available code FEMFAT has been used for fatigue analyses. The code works with other analysis programs rather easily. It is necessary to provide the code with the following information for endurance strength limit analyses:

- **Analysis model**

  The finite element model data is required in order to subsequently calculate stress gradients between neighboring nodes. The calculated stress levels and the relative stress gradient form the basis for consideration of the notch effects, which can have a critical influence on the S/N curve under consideration [14]. The results from the structural analysis are imported to FEMFAT code for required geometrical data and overall load condition as ABAQUS odb file.

- **Load cycle**

The current stress state at each node under consideration is of critical importance for operational strength analyses. Besides the mean stress, the amplitude stress can be taken into consideration for the analysis, allowing for the 3-dimensional stress tensor [14]. Upper and lower stress levels are determined by selecting related steps of the structural analysis. Force – moment step has been selected for upper and gravity step has been selected for lower stress level in this case. This constitutes very severe load cycle where system is subject to load variations between extreme wind load case to no-load dead weight case.

- **Material data**

A number of material data must be defined for operational strength analyses in order to correctly document the dynamic strength behavior of the material. There are several ways to do it. The simplest way to import the material data from the material database in material file format. If no appropriate material file is available, but all material data necessary for analysis is known, the information may also be entered interactively [14].

- **Assigning characteristics to nodes**

Analysis of damage, or endurance limit or static overload safety factors, is generally carried out at the entity nodes. In order to have the relevant influence parameters considered, they must be specified beforehand for the individual nodes. Material data which is defined earlier is assigned to relevant group of nodes [14]. Besides, there are some parameters to enter such as surface roughness, effective size and range of dispersion. Effective size is the relevant wall thickness. Range of dispersion is defined as the ratio of component fatigue strength at 10% survival probability to 90%. Cast hub surfaces are relatively rough. Therefore, surface

roughness values are selected as 250 µm and 500 µm for two different cases. Effective size is calculated as;

$$d_{eff} = \frac{4 * Volume}{Surface\ Area} \tag{6.1}$$

It is calculated as 102.006 by determining volume and surface area of hub from mass properties in SolidWorks. Range of dispersion is used as default number which is 1.26.

- **Selecting the proper analysis procedure**

FEMFAT provides a number of procedures which can be individually selected by the user for calculating influence factors such as damage, endurance safety factor, static safety factor and stress/strain comparison. Endurance safety factor is suitable for the case because no load spectra are necessary for calculating the endurance limit safety factor and it is selected [14].

6.4. Fatigue Analysis Results

Four different fatigue analyses have been conducted for two different scenarios and two different surface roughness values. Surface roughness is different for different regions of hub. Therefore, two different analyses have been conducted to evaluate upper and lower limits.

6.4.1. First Scenario with 250 µm Surface Roughness (#1)

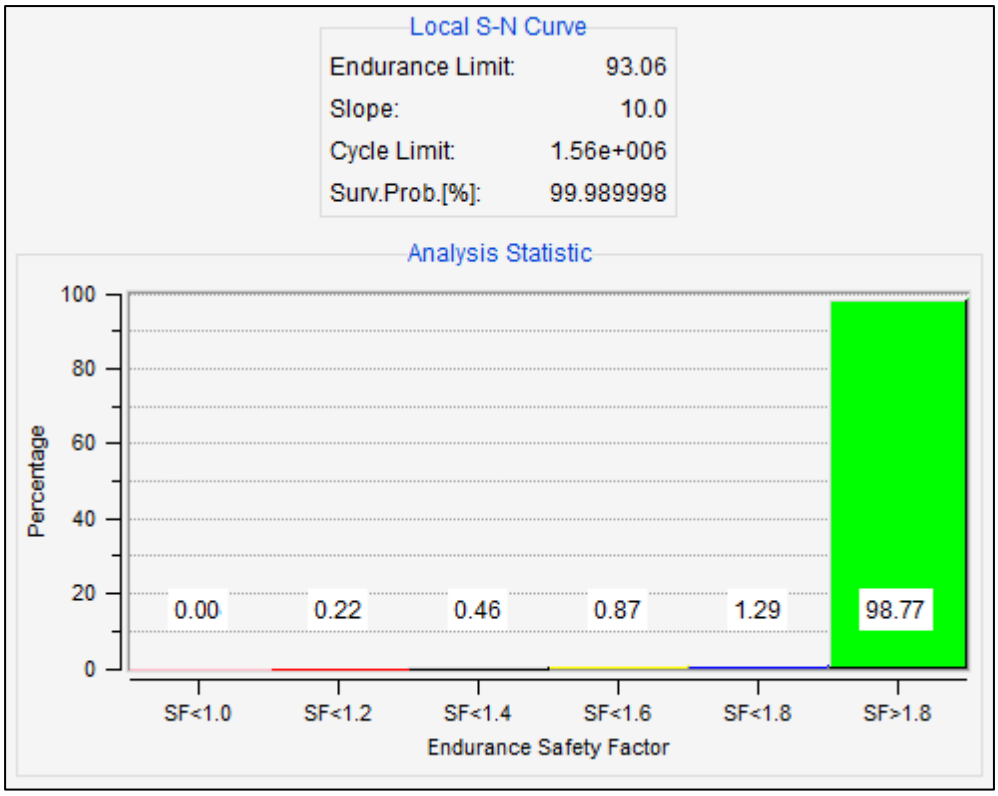

Figure 6.1. Safety Factor Chart for Fatigue Analysis #1

Figure 6.1 demonstrates that most of the part is safe against fatigue. Only 0.22% of the part has safety factor between 1 and 1.2. These areas should be examined for crack propagation. Moreover, cycle limit is 1.56e6 according to analysis results. In other words, such number of cycles to occur from extreme load to none, before local factor of safety reduces below 1.2.

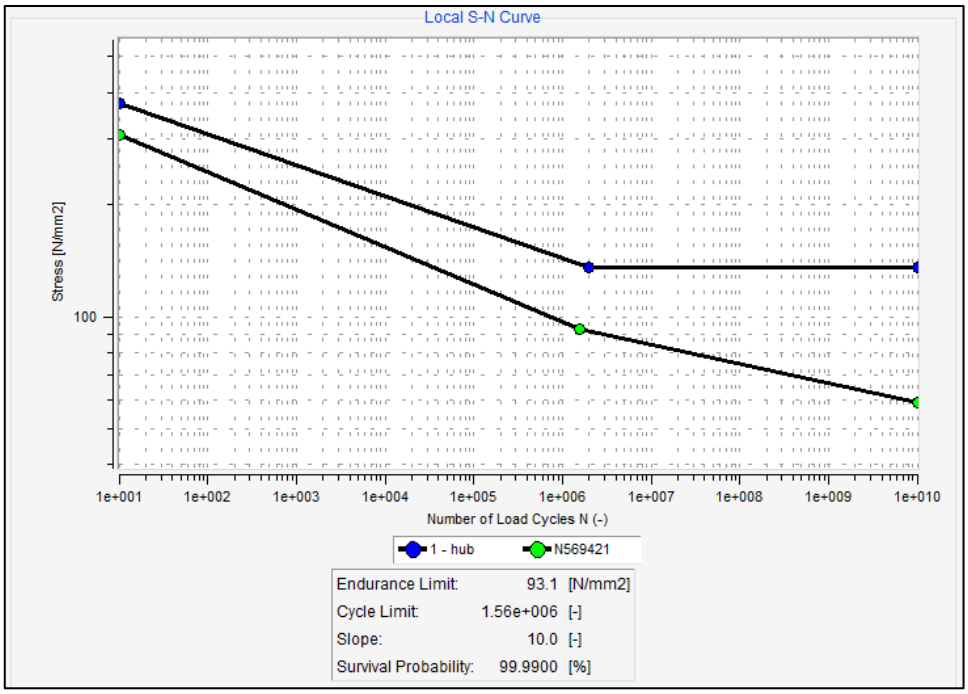

Figure 6.2. S-N curve for Fatigue Analysis #1

This curve was created for the most critical node at the hub part by FEMFAT software. The S-N curve of the most critical node is totally under the hub's S-N curve as it is in Figure 6.2.

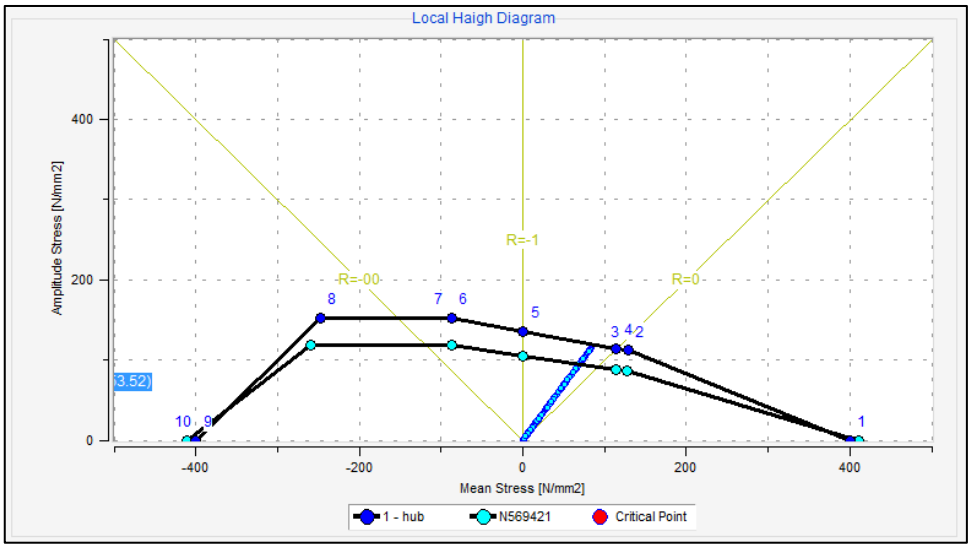

Figure 6.3. Haigh Diagram for Fatigue Analysis #1

Figure 6.3 shows local Haigh diagram of the hub part with respect to Fatigue Analysis #1. Critical nodes are in the convex curve of the part's diagram. In other words, there is no critical nodes which is not safe.

Critical regions are around the weight reduction and man holes as it is seen in Figure 6.4. Safety factor limit is set to 1.1 safety factor to be conservative. Other areas generally have much higher safety factor values up to 20. However, man holes are risky areas as it is in structural analysis.

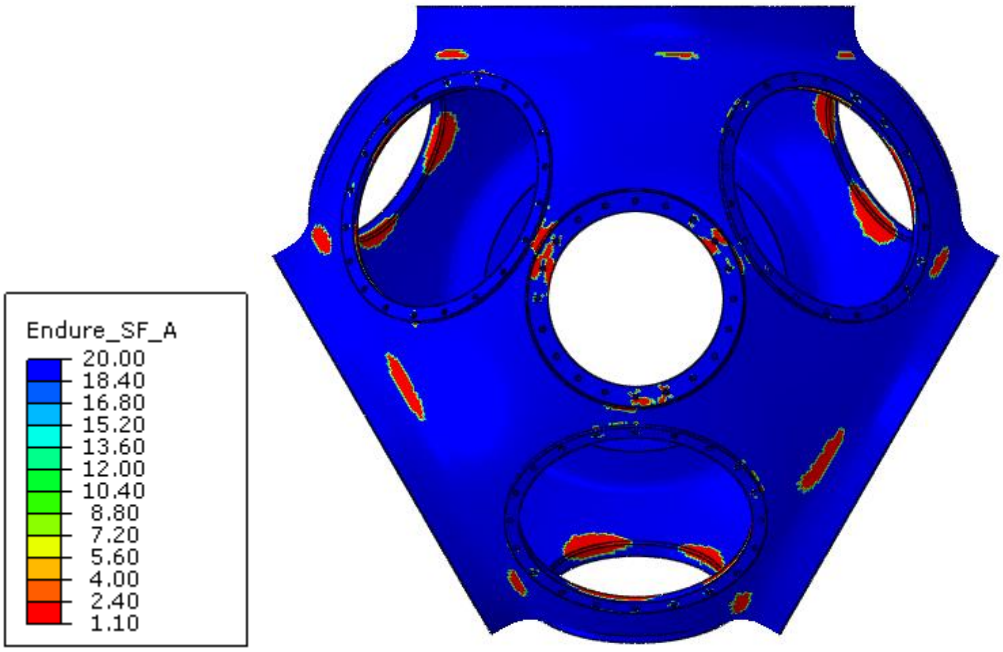

Figure 6.4. Endurance Safety Factor for Fatigue Analysis #1

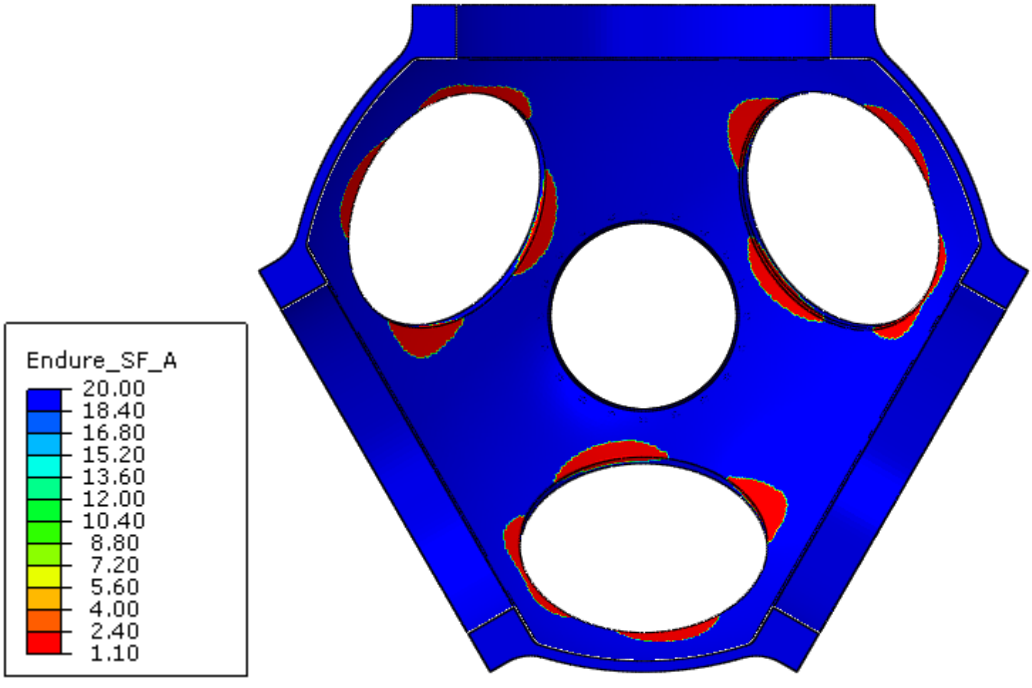

Figure 6.5. Endurance Safety Factor for Fatigue Analysis #1

6.4.2. First Scenario with 500 µm Surface Roughness (#2)

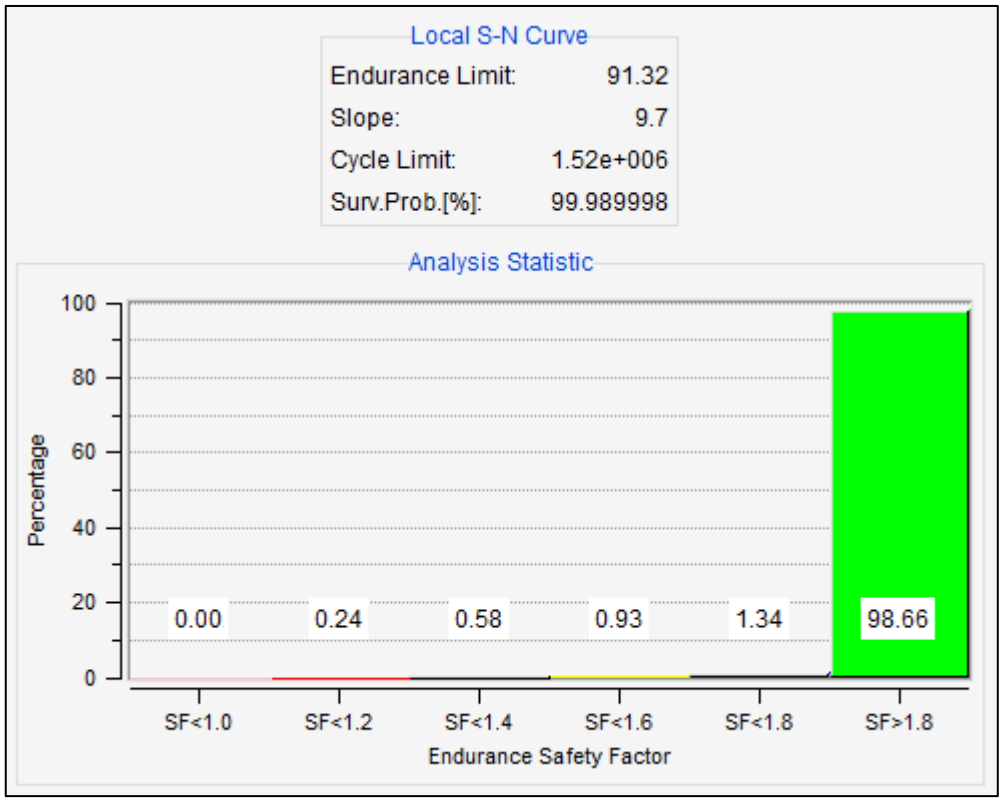

Figure 6.6. Safety Factor Chart for Fatigue Analysis #2

Figure 6.6 demonstrates that most of the part is safe against fatigue. Only 0.24% of the part has safety factor between 1 and 1.2. There areas should be examined for crack propagation. Moreover, cycle limit is 1.52e6 according to analysis results. In other words, such number of cycles to occur from extreme load to none, before local factor of safety reduces below 1.2.

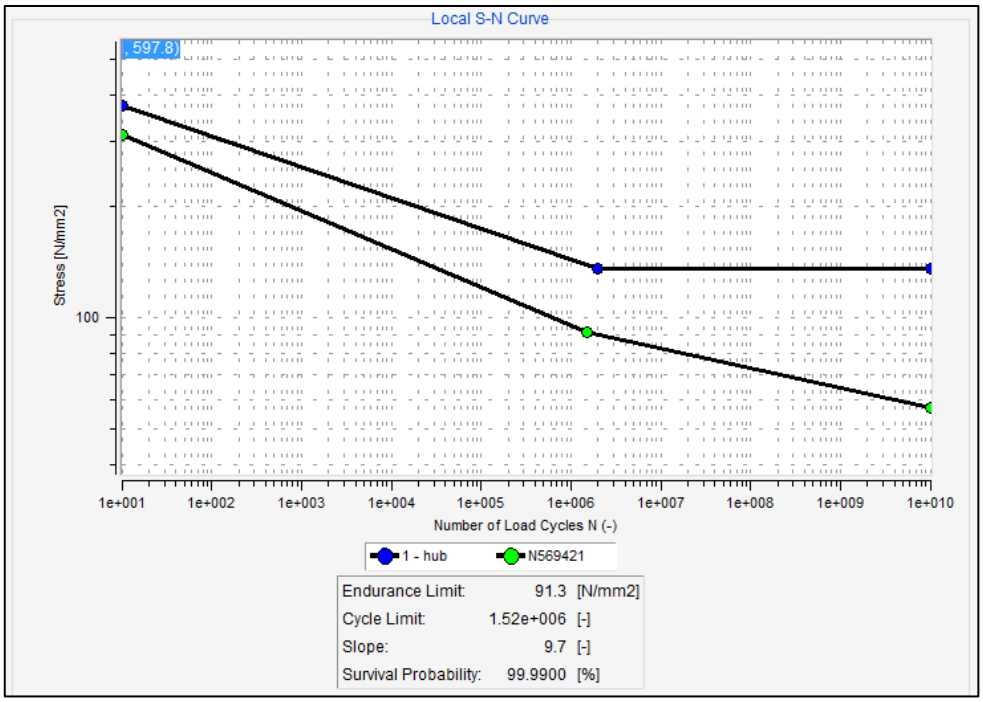

Figure 6.7. S-N curve for Fatigue Analysis #2

This curve was created for the most critical node at the hub part by FEMFAT software. The S-N curve of the most critical node is totally under the hub's S-N curve as it is in Figure 6.7.

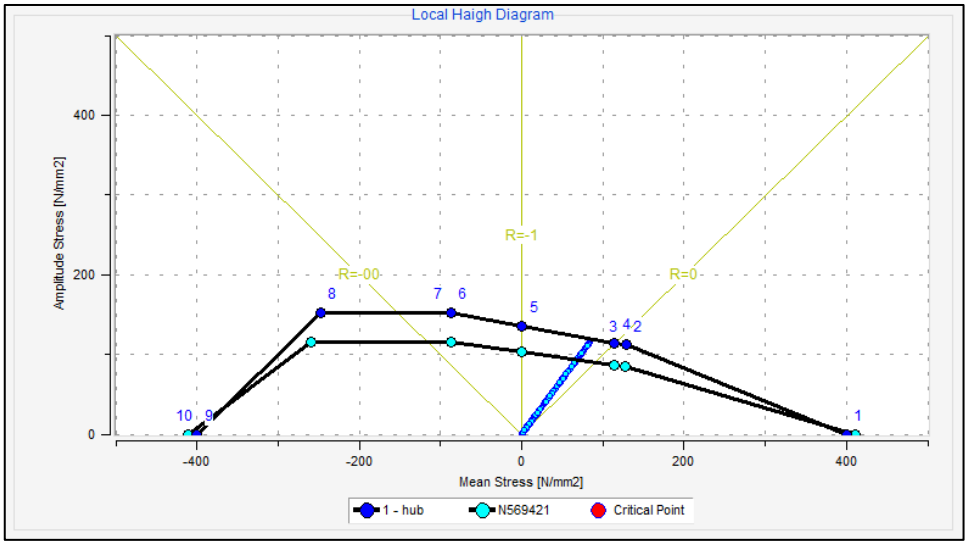

Figure 6.8. Haigh Diagram for Fatigue Analysis #2

Figure 6.8 shows local Haigh diagram of the hub part with for the Fatigue Analysis #2. Critical nodes are in the convex curve of the part's diagram. In other words, there is no critical nodes which is not safe.

Critical regions are around the weight reduction and man holes as it is seen in Figure 6.9 and Figure 6.10. Safety factor limit is set to 1.1 safety factor to be conservative. Other areas generally have much higher safety factor values up to 20. However, man holes are risky areas as also observed in structural analysis.

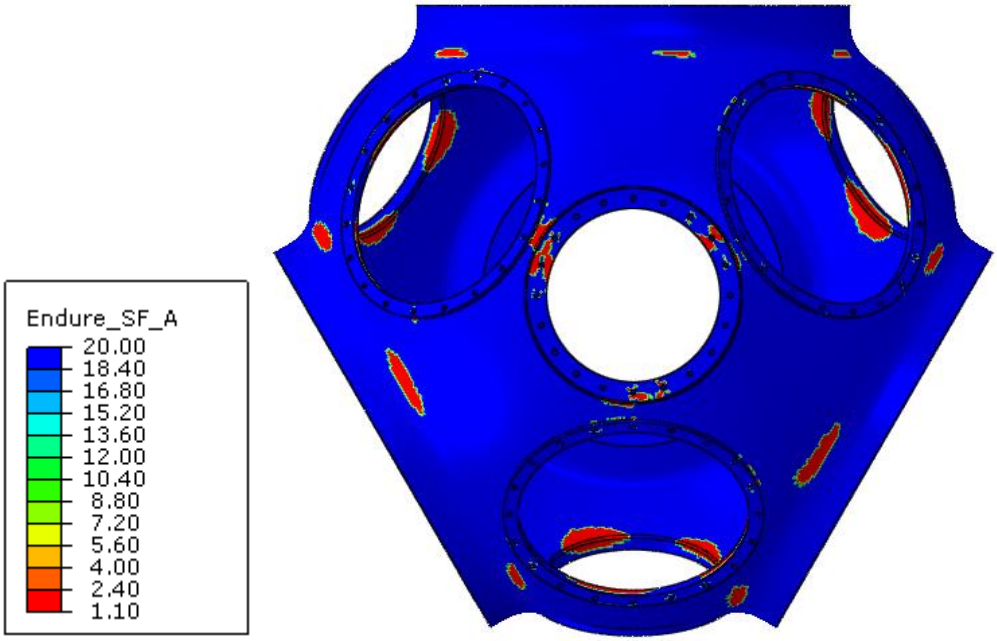

Figure 6.9. Endurance Safety Factor for Fatigue Analysis #2

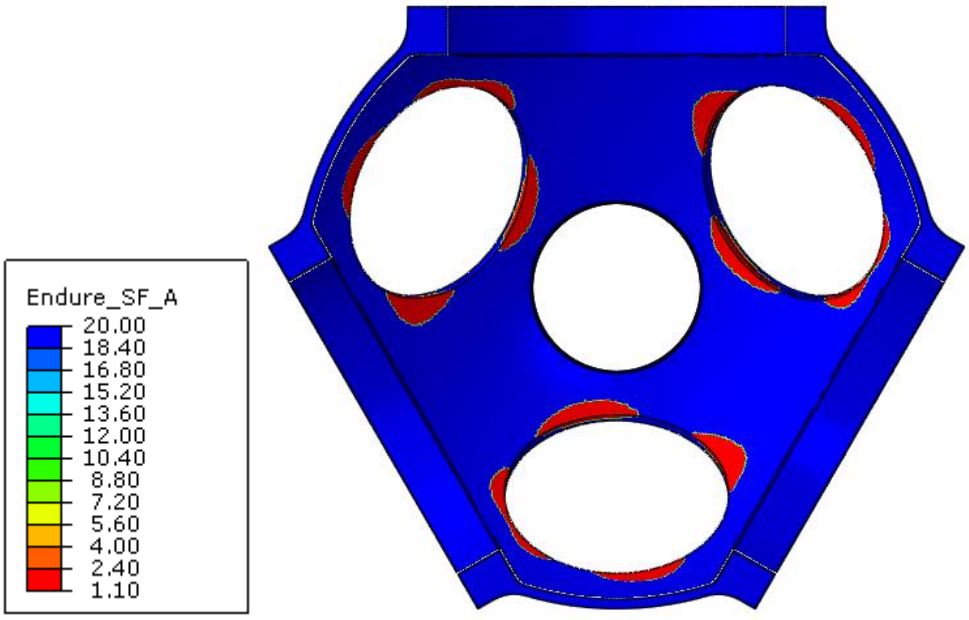

Figure 6.10. Endurance Safety Factor for Fatigue Analysis #2

6.4.3. Second Scenario with 250 µm Surface Roughness (#3)

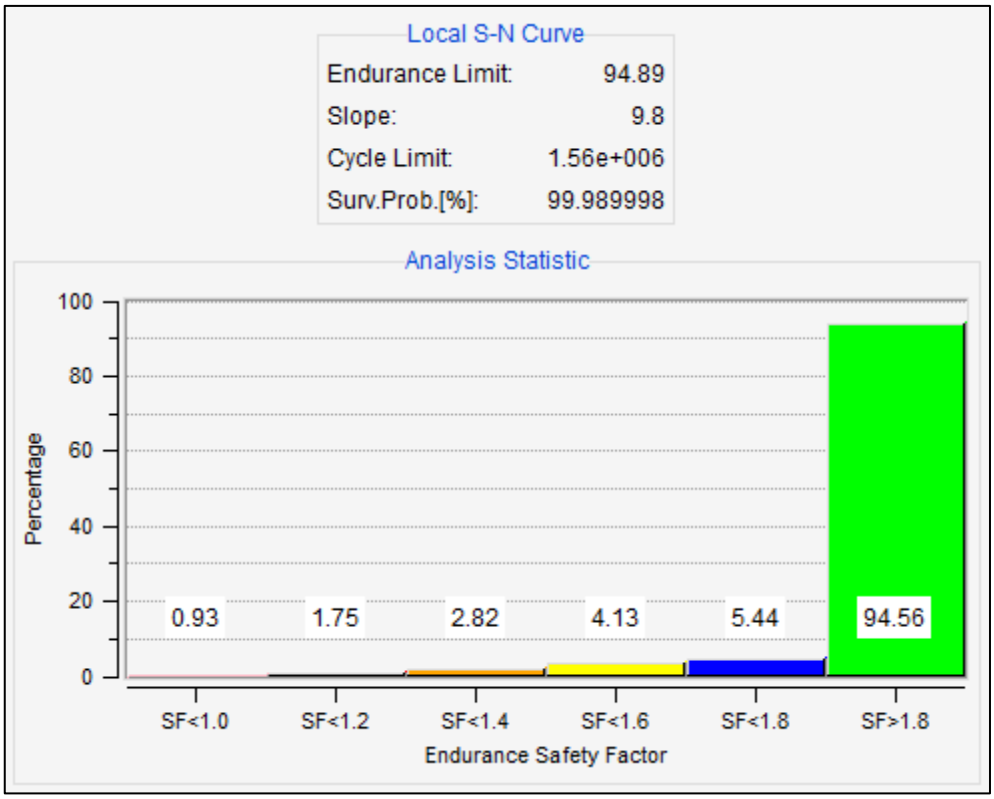

Figure 6.11. Safety Factor Chart for Fatigue Analysis #3

Figure 6.11 demonstrates that although most of the part is safe against fatigue, 0.93% of the part has safety factor less than 1. These areas should be examined for crack propagation. Moreover, cycle limit is 1.56e6 according to analysis results. In other words, such number of cycles to occur from extreme load to none, before some damage to the part.

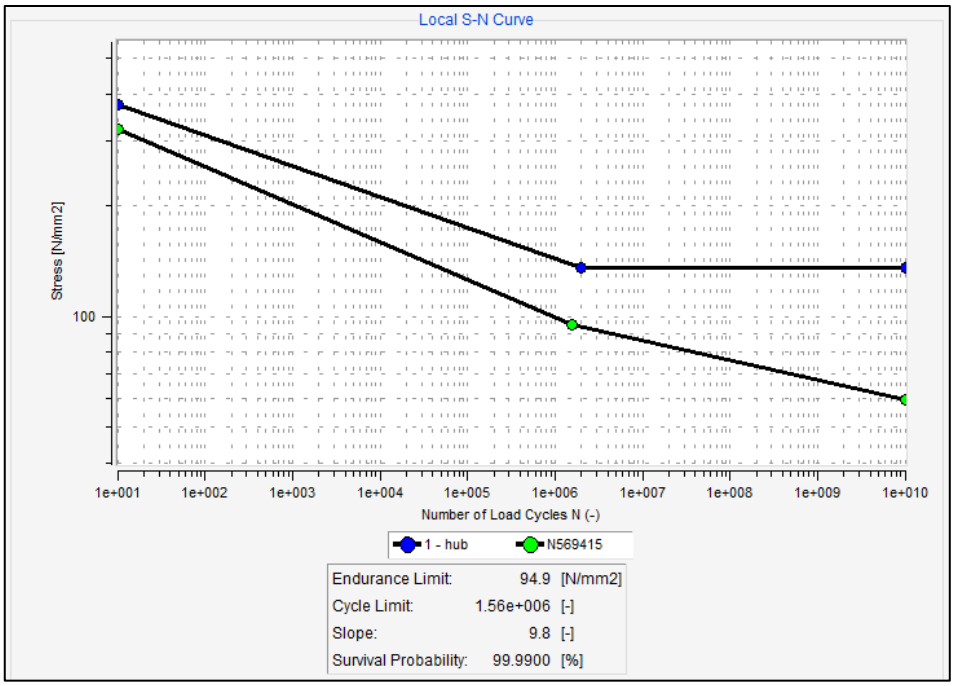

Figure 6.12. S-N curve for Fatigue Analysis #3

This curve was created for the most critical node at the hub part by FEMFAT software. The S-N curve of the most critical node is totally under the hub's S-N curve as it is in Figure 6.12.

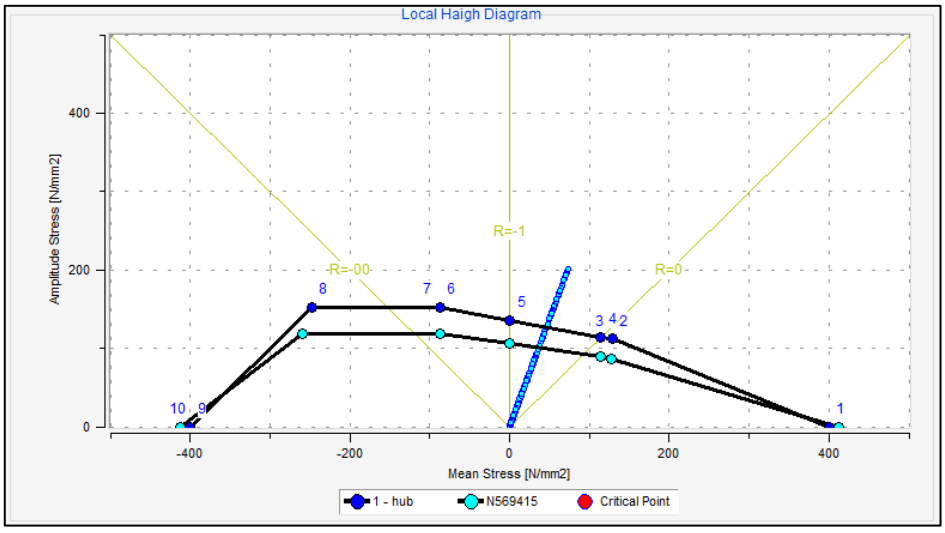

Figure 6.13. Haigh Diagram for Fatigue Analysis #3

Figure 6.13 shows local Haigh diagram of the hub part with respect to Fatigue Analysis #3. Some of the nodes are out of the hub's diagram. This means that there are some critical nodes which are not safe.

Critical regions are around the weight reduction and man holes and some other areas on outer surface as it is illustrated in Figures 6.14 and 6.15. Safety factor limit is set to 1.1 safety factor to be conservative. Other areas generally have much higher safety factor values up to 10. There are much more areas at this analysis than analyses which are made with the first scenario.

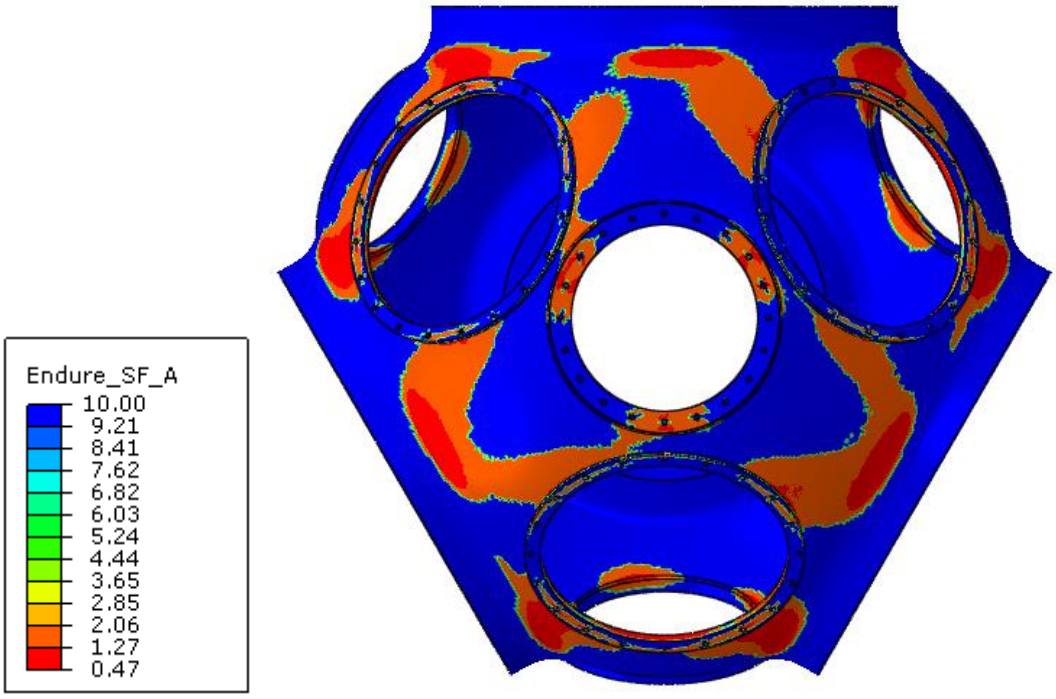

Figure 6.14. Endurance Safety Factor for Fatigue Analysis #3

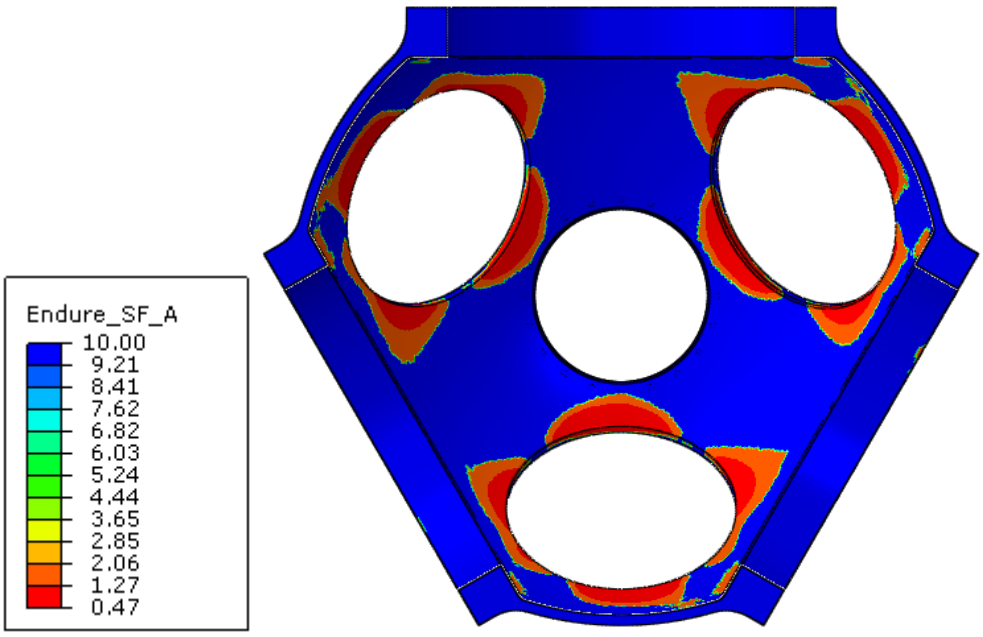

Figure 6.15. Endurance Safety Factor for Fatigue Analysis #3

6.4.4. Second Scenario with 500 µm Surface Roughness (#4)

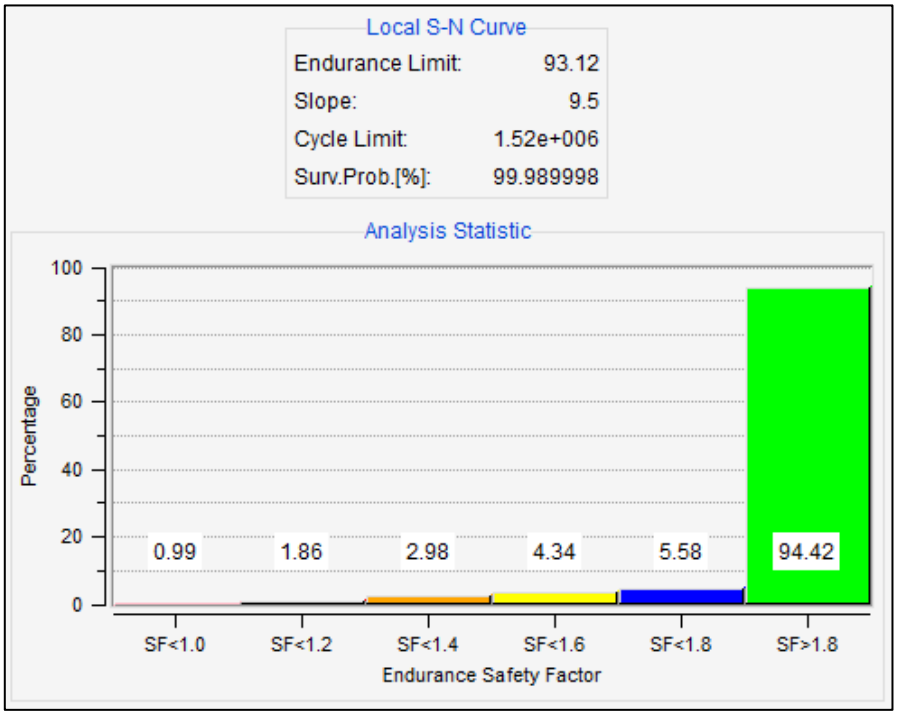

Figure 6.16. Safety Factor Chart for Fatigue Analysis #4

Figure 6.16 demonstrates that although most of the part is safe against fatigue, 0.99% of the part has safety factor less than 1. There areas should be examined for crack propagation. Moreover, cycle limit is 1.52e6 according to analysis results. In other words, such number of cycles to occur from extreme load to none, before some damage to the part.

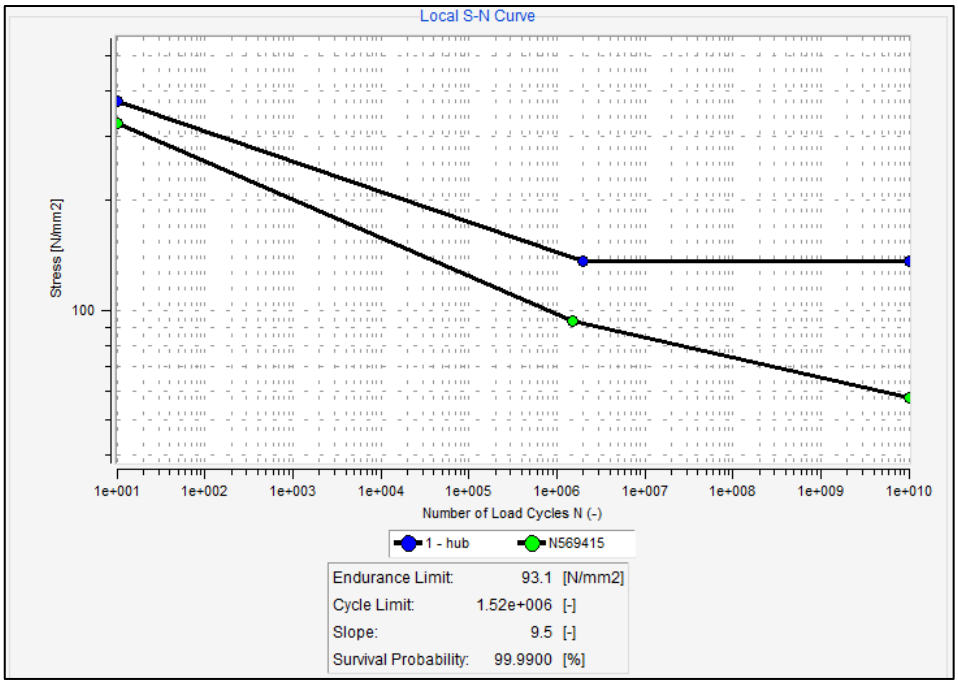

Figure 6.17. S-N curve for Fatigue Analysis #4

This curve was created for the most critical node at the hub part by FEMFAT software. The S-N curve of the most critical node is totally under the hub's S-N curve as it is in Figure 6.17.

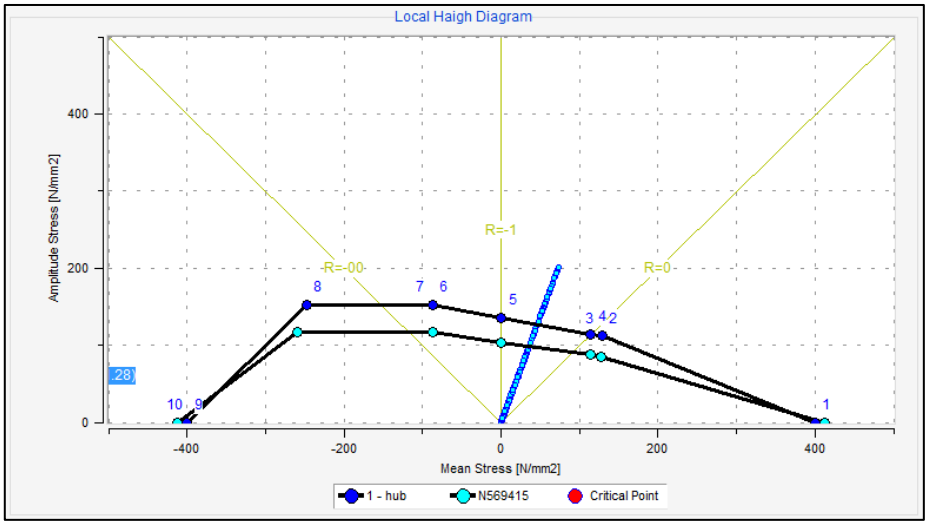

Figure 6.18. Haigh Diagram for Fatigue Analysis #4

Figure 6.18 shows local Haigh diagram of the hub part with respect to Fatigue Analysis #4. Some of the nodes are out of the hub's diagram. This means that there are some critical nodes which are not safe.

Critical regions are around the weight reduction and man holes and some other areas on outer surface as it is presented in Figures 6.19 and 6.20. Safety factor limit is set to 1.1 to be conservative. Other areas generally have much higher safety factor values up to 10. There are much more critical areas in this analysis than analyses indicate for the first scenario.

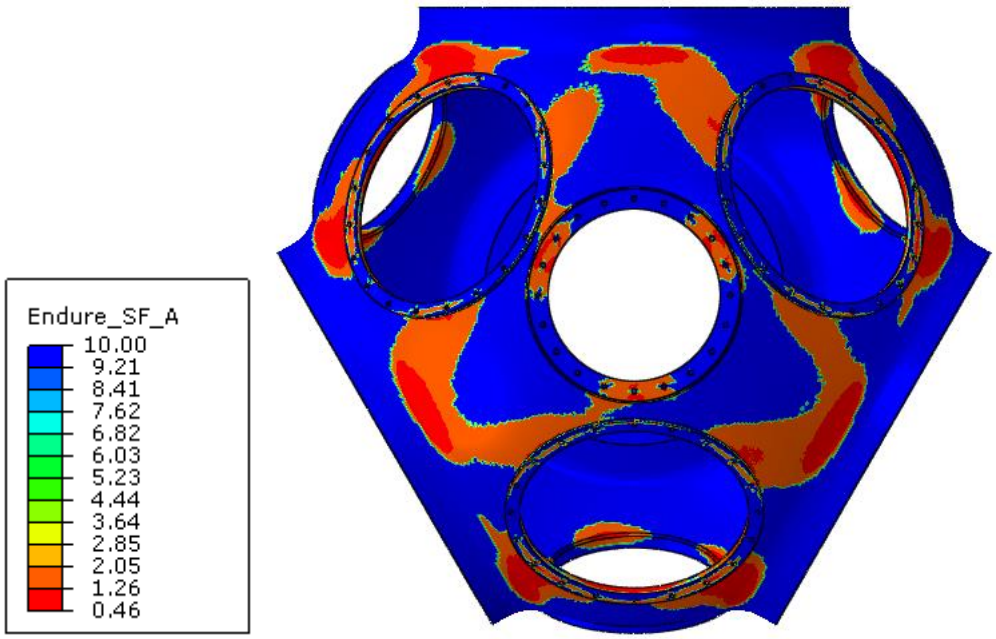

Figure 6.19. Endurance Safety Factor for Fatigue Analysis #4

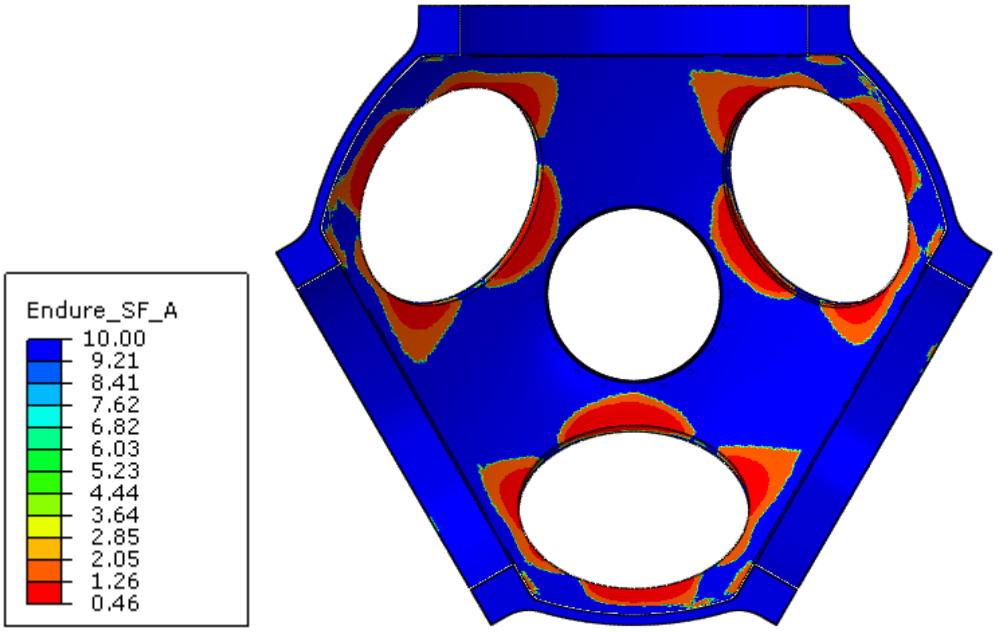

Figure 6.20. Endurance Safety Factor for Fatigue Analysis #4

6.5. Discussion on Fatigue Analysis Results

As observed from analysis results, for the evaluated load cases some hub regions especially around weight reduction and man holes are critical. Both of the loading scenarios (-8 degree pitch angle and 32 degree pitch angle) represent extreme cases which are unlikely to occur during regular wind turbine operation. Typical wind turbine operation occurs between 0 to 16 degree pitch angle. 32 degree pitch angle represents an occasional case where turbine is speeding up under low wind conditions. However, moments and forces that are used in both load scenarios represent 60 years worst wind gust condition. Therefore, combination of such a pitch angle and wind level is not possible, as under such gust conditions turbine is not operational and in park position. Similar arguments may be said for -8 degree pitch angle case. However, these two cases have been picked as the worst possible load condition case among many different pitch angle ranges. The reason for the analyses to be performed using these two extreme cases is not to determine fatigue factor of safety, rather to identify critical regions for fatigue failure during experimental operation of the prototype. These locations will be equipped with strain gauges and their load cycles will be closely monitored until the design is validated.

7. CONCLUSION

In this work, hub component of a 500 kW wind turbine has been analyzed. First, its finite element model has been created based on its 3D design. Then, HyperMesh software has been utilized to create detailed and homogeneous model mesh. Material information has been added to the model. All contacts have been defined in ABAQUS. Gravity, force and moment loadings have been added to the model. Finally, model has been analyzed via finite element solver ABAQUS.

Stress values and contacts have been examined carefully. Structural analysis results are presented in Table 5.6. Analyses indicate that -8 degree blade pitch condition presents the worst case conditions. There are local failures near weight reduction and man holes. Evaluation of contact forces indicate that all contacts have sufficient friction and bolt load levels.

Fatigue analyses are conducted using FEMFAT. Similar to structural analyses second load scenario with -8 degree blade pitch condition presents the worst case conditions. Analyses indicate that fatigue failure and crack propagation is possible near weight reduction and man holes. Although both load conditions represent unlikely combinations, it is recommended that dimensions of man holes may be reduced or wall thickness of the hub may be increased to reduce failure risk at such areas. All the critical areas for fatigue failure have been identified. These regions should be monitored during experimental operation until the design is validated.

REFERENCES

[1] Hansen, M., Aerodynamics of Wind Turbines 2nd edition, 2008.

[2] Durak, M., 2009 Yılı Sonu İtibarı İle Dünya'da ve Ülkemizde Rüzgar Elektrik Santral (RES) Projelerinin Son Durumu, TÜREB 2010, 2009.

[3] Altuntaşoğlu, Z., Yerli Rüzgar Enerji Teknoloji Üretimi Destek Politikaları, İstihdam Olanakları ve Türkiye'deki Durum, Mühendis ve Makine Dergisi, Sayı: 5942008, 1999.

[4] Malkoç, Y., Türkiye Rüzgar Enerjisi Potansiyeli ve Enerji Profilimizdeki Yeri, it is taken from http://www.solar-academy.com/menuis/Turkish-Wind-Data.023202.pdf on 10.07.2014.

[5] Demir, S., Rüzgar Türbini Göbeği İmalatı ve Sistem İntegrasyonu, Kocaeli Üniversitesi, 2013.

[6] Johnson, L. G., Wind Energy Systems, 2001.

[7] Burton, T., Sharpe, D., Jenkins, N., Bossanyi, E., Wind Energy Handbook, 2001.

[8] It is taken from http://www.teachergeek.org/wind_turbine_types.pdf on 13.07.2014.

[9] Fink, D., Energy Self Sufficiency Newsletter, August 2005.

[10] It is taken from http://www.thesolarguide.com/wind-power/turbine-parts.aspx on 13.07.2014.

[11] Stiesdal, H., Wind Turbine Components and Operation, Bonus Energy A/S, Bonus Info Specia Issue, (1999).

[12] Shirani, M., Harkegard, G., "Fatigue life distribution and size effect in ductile cast iron for wind turbine components", Engineering Failure Analysis, S1350-6307(10)00127-5, (2010)

[13] Yaşar, M. , "Dizel otomobil pompa milinin yorulma kırılması analizi", Proceedings of 8th International Fracture Conference (2007)

[14] FEMFAT 5.0 – BASIC User Manual, 2011.

[15] Muhammad, A., Ristow, M., Fatigue Life of Wind Turbine Structural Components, November 2010, NAFEMS Seminar, Hamburg, Germany.

[16] Goezinne, F., Technical Calculations, October 1991.

[17] Roylance, D., "Fatigue", Department of Materials Science and Engineering Massachussetts Institute of Technology Cambridge, (2001).

[18] Robert, L. Norton, Mechanical Engineering Design, 5th Edition, 2010.

[19] Shigley's, Richard, G., Mechanical Engineering Design, 9th Edition, 2011.

[20] Malcolm, D.J., Hansen, A.C., “Rotor Design Study”, US Department of Energy, NREL/SR-500-32495, (2006).